Title: **Syntaxin11 Deficiency Inhibits CRAC Channel Priming To Suppress Cytotoxicity And Gene Expression In FHLH4 Patient T Lymphocytes.**

Sritama Datta[1], Abhikarsh Gupta[1#], Kunal Mukesh Jagetiya[1#], Vikas Tiwari[2⊥], Megumi Yamashita[3⊥], Sandra Ammann[4,5], Mohammad Shahrooei[6], Atharva Rahul Yande[1], Ramanathan Sowdhamini[2], Adish Dani[1], Murali Prakriya[3], Monika Vig[1*]

Address and Affiliation: [1]Tata Institute of Fundamental Research, Hyderabad, India. [2]National Centre for Biological Sciences, Bangalore, India. [3]Northwestern University, Feinberg School of Medicine, Chicago, USA. [4]Institute for Immunodeficiency, Center for Chronic Immunodeficiency, Medical center, University of Freiburg, Faculty of Medicine, University of Freiburg, Freiburg, Germany. [5]Institute for Transfusion Medicine and Gene Therapy, Medical Center, University of Freiburg, Faculty of Medicine, University of Freiburg, Freiburg, Germany. [6]Department of Microbiology, Immunology and Transplantation, Clinical and Diagnostic Immunology, KU Leuven, Leuven, Belgium.

[#, ⊥] These authors contributed equally.

***Correspondence to:** monika.vig@gmail.com

Keywords: Orai, Stim, SNAP, SNARE, CRAC, Syntaxin11, ion channels, SOCE, FHLH4, autoimmunity, cytotoxicity, CTL, T lymphocytes

Abstract:

CRAC channels enable calcium entry from the extracellular space in response to a variety of stimuli and are crucial for gene expression and granule exocytosis in lymphocytes. Here we find that Syntaxin11, a Q-SNARE, associated with FHLH4 disease in human patients, directly binds Orai1, the pore forming subunit of CRAC channels. Syntaxin11 depletion strongly inhibited SOCE, CRAC currents, IL-2 expression and cytotoxicity in cell lines and FHLH4 patient T lymphocytes. Constitutively active H134 Orai1 mutant completely reconstituted calcium entry in Syntaxin11 depleted cells and the defects of granule exocytosis as well as gene expression could be bypassed by ionomycin induced calcium influx in FHLH4 T lymphocytes. Our data reveal a Syntaxin11 induced pre-activation state of Orai which is necessary for its subsequent coupling and gating by the endoplasmic reticulum resident Stim protein. We propose that ion channel regulation by specific SNAREs is a primary and conserved function which may have preceded their role in vesicle fusion.

Introduction:

Most eukaryotic cells have a limited amount of calcium sequestered inside intracellular stores, the largest of which are the endoplasmic reticulum (ER). Signaling from cell surface receptors induces the release of stored calcium which, in turn, activates store-operated calcium entry (SOCE) to replenish the stores and sustain signaling and other calcium dependent cellular processes [1]. Calcium release activated calcium (CRAC) channels play a major role in mediating SOCE [2]. In lymphocytes and mast cells, CRAC currents have been shown to be crucial for granule exocytosis as well as gene expression associated with effector functions [3 4 5]. Orai (CRACM) multimers form the pore of CRAC channels [6] and ER-resident Stim proteins sense store-depletion and subsequently trap and gate freely diffusing resting Orai in ER-PM junctions [7]. CRAC channels are therefore thought to be dependent on Stim proteins for any structural transitions that result in the activation of CRAC currents [8].

Genome-wide RNAi screens, which initially identified Stim and Orai [9-13], have yielded a wealth of information regarding additional players in SOCE. For instance, we have previously shown that alpha-soluble N-ethylmaleimide sensitive factor (NSF) attachment protein (α-SNAP), a well-known synaptic family adaptor protein that forms a part of the 20S SNARE super-complex[14, 15], is a crucial component of the CRAC channel supramolecular complex [12, 16]. α-SNAP independently bound Stim as well as Orai, with high affinity [17-19]. Single particle diffusion analysis showed that store-depletion induced arrest of Orai mobility was completely reversed in α-SNAP depleted cells, suggesting non-functional co-clustering with Stim proteins [17]. Step-photobleaching analysis of Orai1 further showed altered stoichiometry and ion selectivity of Orai1 multimers in α-SNAP depleted cells demonstrating that α-SNAP is required for the on-site assembly and ion selectivity of CRAC channels [17]. Therefore, analysis of the role of α-SNAP revealed that Stim:Orai coupling is necessary but not sufficient for SOCE and the molecular process likely involves multiple additional steps.

A key question related to the above described findings is whether and how do the additional molecular players of the synaptic machinery regulate SOCE? Our previous analyses have shown that alpha-SNAP functions independently of its usual binding partner NSF-ATPase in the regulation of SOCE [16]. However, this question remains incompletely addressed and becomes even more pertinent because specific SNAREs appeared in two independent genome-wide RNAi screens previously conducted in *Drosophila* cells to identify regulators of SOCE but were not characterized [11, 12]. Additionally, associations of SNAREs with pore-forming subunits of a variety of channels have been reported previously, however, several of these interactions were reported to be inhibitory [20 21]. In others, SNAREs were initially thought to be required for the insertion of pore subunits into the target membrane [22-24]. Several earlier reports documenting the direct association of VGCCs with t-SNAREs have proposed that interactions with synaptic machinery serve to localize the source of calcium influx close to the sites of secretory and synaptic vesicle fusion. However, this hypothesis runs into following problems. First, SNAREs also associate with the pore subunits of potassium (Kv2.1), chloride (CFTR) and sodium channels, neither of which conduct calcium to facilitate membrane fusion [25-28]. Second, recent studies have identified several other adaptor proteins such as calcium-calmodulin dependent serine kinase (CASK) and Mint-1, which directly bind Cav channels and could serve the function of anchoring at desired locations [22]. Finally, synaptic proteins should not have to bind close to the pore forming region, in order to perform the task of anchoring the channels. Therefore, the exact role of these associations remains unestablished, but a common theme that emerges is that none of them directly modulate the surface expression of the candidate channels [16, 25, 26, 29, 30]. Furthermore, SNAREs are highly expressed proteins in most cells [23], yet only three assembled SNARE complexes are needed for the fast fusion exocytosis in chromaffin cells [31] and two synaptobrevin molecules are sufficient for vesicle fusion in hippocampal neurons [32].

It is therefore necessary to envisage an alternate, and more fundamental, function for the association of SNAREs with the ion channel pore subunits. We hypothesized that additional synaptic proteins are involved in the direct regulation of SOCE. However, because the repertoire of synaptic family proteins is much larger in mammalian cells, we

conducted a limited RNAi screen in HEK293 and Jurkat T cells, where we initially targeted those synaptic family genes that are expressed in both cells. STX11 specifically regulated SOCE, gene expression and cytolysis by directly binding to Orai and inducing a hitherto unsuspected, early molecular transition which prepared Orai for subsequent gating by Stim. Further, defective SOCE drove the granule exocytosis defects of STX11 deficient FHLH4 patient T lymphocytes, which could be bypassed with ionomycin.

Results:

We have previously shown that α-SNAP, a ubiquitously expressed synaptic family protein, forms an integral component of the functional CRAC channel complex and binds Orai1 and Stim1 with high affinity [12, 16 17-19]. NSF-ATPase, a usual binding partner of α-SNAP, was not involved in regulating SOCE [16]. However, α-SNAP also binds the cis-SNARE complex and a Q-SNARE, Syntaxin 5 (STX5), showed inhibition of SOCE in one of the earlier genome-wide screen performed in *Drosophila* S2 cells [11]. Furthermore, STX1 has been previously shown to bind a variety of ion channels [22-24]. Therefore, to assess the potential role of Syntaxins in SOCE, we first knocked down STX5 (Supplementary Figure 1A) and STX1A (Supplementary Figure 1B) using five different sequences of shRNA targeting each gene in HEK293 cells and measured SOCE in response to Thapsigargin (TG). We did not see a significant defect in SOCE in either of the cases. However, several members of the synaptic family proteins are not ubiquitously expressed and many show redundancy in their function. Therefore, we searched online databases and initially only targeted synaptic family protein genes that are expressed in HEK293 and T cells (Supplementary Figure 1C-N). We found that Syntaxin11 knockdown showed strong inhibition of SOCE in a variety of cell lines (Supplementary Figure 1D) (Figure 1A-F). To establish specificity of the knockdown, we expressed STX11 in STX11 depleted cells, which largely restored SOCE (Figure 1G). In addition, we knocked down STX11 using an additional shRNA sequence, which also significantly inhibited SOCE in Jurkat T cells (Supplementary Figure 2). To assess the extent of STX11 mRNA depletion, we extracted total RNA from scramble (scr) and STX11 shRNA treated HEK293 cells and subjected it to quantitative PCR analysis using Taqman probes (Supplementary Figure 3). We observed nearly 70% depletion of STX11 mRNA. To determine whether ectopic expression of STX11 would enhance SOCE, we expressed STX11 in HEK293 (Figure 1H) and Jurkat T cells (Supplementary Figure 4) and measured SOCE. There was a significant increase in both the cases reinforcing a crucial role of STX11 in SOCE. To determine whether the increase in SOCE seen upon the expression of STX11 was due to CRAC channels, we depleted Orai1 expression before expressing STX11 in HEK293

cells. The STX11 mediated enhancement observed in SOCE was lost in Orai1 depleted cells (Figure 1I).

Previous studies have shown that SOCE in T cells is mediated by CRAC channels formed by Orai proteins. To test whether CRAC current (I_{CRAC}) is affected by knockdown of STX11 in T cells, we performed whole cell patch clamp recordings on scramble (scr) and STX11 shRNA treated Jurkat T cells (Figure 2A-C). Leak-subtracted I_{CRAC} was recorded in 20 mM Ca^{2+} and a Na^{+}-based divalent cation free (DVF) solution. These recordings showed that both the Ca^{2+} and DVF CRAC current is decreased more than two-fold in the STX11 shRNA treated cells with the normalized currents shown in Figure 2C. The electrophysiological properties of the residual current in STX11 shRNA treated cells was indistinguishable from I_{CRAC} in scramble shRNA treated cells in terms of blockade of the Ca^{2+} current by La^{3+}, depotentiation of the DVF current over tens of seconds, and fast inactivation of Ca^{2+} current. Moreover, the reversal potential of the $Ca^{2+}$and DVF currents were similar between scramble and STX11 shRNA treated Jurkat T cells, suggesting that STX11 depletion does not affect the calcium selectivity of CRAC channels (Figure 2D). These results indicate that knockdown of STX11 significantly decreases I_{CRAC} in Jurkat T cells.

CRAC channel mediated calcium influx is crucial for sustained calcium signaling which, in turn, is required for the activation and nuclear translocation of specific transcription factors such as nuclear factor of activated T (NFAT) [2] [33]. We stimulated control and STX11 depleted Jurkat T cells with thapsigargin (TG) and phorbol myristate acetate (PMA), prepared nuclear and cytosolic extracts and subjected them to Western blot using anti-NFAT antibody (Figure 2E). The nuclear translocation of NFAT was severely compromised in STX11 depleted T cells. To visualize NFAT translocation in response to T cell receptor mediated stimulation, we incubated control and STX11 depleted Jurkat T cells with plate-coated anti-CD3 and soluble anti-CD28, fixed, permeabilized and immunolabelled for NFAT. Representative images and quantification of the nuclear NFAT fraction (Figure 2F, 2G) across multiple randomly chosen fields shows that STX11 depleted cells are deficient in NFAT nuclear translocation upon anti-

CD3 stimulation. The defect of NFAT translocation also affects gene expression, as assessed by IL-2 specific QPCR of control and STX11 depleted Jurkat cells upon anti-CD3 stimulation (Figure 2H). Taken together, these data demonstrate an essential role for STX11 in SOCE *via* CRAC channels, NFAT activation and gene expression.

STX11 is a Q-SNARE protein and most Q-SNAREs possess a C-terminal transmembrane domain for membrane insertion [34]. However, STX11 is atypical in this regard because it harbors a group of cysteine residues close to the C-terminus in place of the transmembrane domain (Supplementary Figure 5). The cellular localization of STX11 is not established [35] [36] [37]. This is primarily because using the available commercial antibodies, native STX11 is undetectable in most cell lines and tagging STX11 on either the N- or the C-terminus results in partial degradation and mis-localization of the protein (data not shown) [35]. Therefore, to determine its localization in HEK293 cells, we inserted an HA tag inside the N-terminal unstructured region of STX11, just before the beginning of the Habc domain, expressed in HEK cells, permeabilized and labelled with anti-HA tag antibody. STX11 with an internal HA tag localized in the plasma membrane (Figure 3A). We next expressed untagged STX11 in cells co-expressing Orai1-YFP, permeabilized and stained with anti-STX11 antibody. In majority of cells, STX11 co-localized with Orai1 in the plasma membrane (Figure 3B). Co-localization of STX11 and Orai1 suggested a direct role in SOCE. To test this, we co-expressed STX11 with either Flag- or Myc-tagged Orai1 in HEK293, prepared whole cell lysates and subjected them to co-immunoprecipitation followed by Western Blot using either anti-Flag, anti-Myc or anti-STX11 antibodies. We found that both Orai1 and STX11 could co-immunoprecipitate each other under resting as well as store-depleted conditions (Figure 3C, 3D). To further assess whether STX11 directly binds Orai1, we expressed and purified from *E. Coli*, MBP-tagged N- and C-terminal cytosolic tails of Orai1 (Figure 3E). *In vitro* pull-down assay performed by incubating Orai1 cytoplasmic domains with full length soluble His-tagged STX11 showed that both the N-terminus as well as the C-terminus of Orai1 bound STX11 albeit with different apparent affinities (Figure 3F). In both cases, the binding of STX11 to Orai1 was similar or higher when compared to SNAP23, a known binding partner of STX11. SNARE proteins typically utilize their SNARE domain for interacting

with other SNAREs [34]. To identify the domain of STX11 involved in the regulation of SOCE, we expressed His-tagged H_{abc} and SNARE domains of STX11 in *E. Coli*, purified and assessed their binding to the MBP-tagged Orai1 tails *via* a similar pull-down assay. We found that the H_{abc} domain of STX11 showed significantly high binding to the C-terminus of Orai1 but faint binding to the N-terminus was also detected (Figure 3G). The SNARE domain did not show any binding to the Orai1 tails but showed faint binding to SNAP23 (Supplementary Figure 6). We analyzed the ability of full length Orai1 and STX11 to form a complex using AlphaFold3 (AF3), however, the scores were insignificant (ipTM = 0.11 and pTM = 0.35). Therefore, we examined domain-domain interactions STX11 (H_{abc}, SNARE) and Orai1 (N-terminus, C-terminus). The complex of STX11 H_{abc} with Orai1 C-terminus resulted in a significantly high prediction score (Supplementary Table 1). The AF3 predictions can vary with different seeds. Therefore, we executed AF3 predictions with different initial seeds to generate multiple models of STX11 H_{abc} with Orai1 C-terminus. The contact frequency of interface residues was calculated in different models. Multiple residues of STX11 H_{abc} domain and Orai1 C-terminus domain were observed to have contact frequency of more than 0.8 (Supplementary Figure 7). The best scoring model among all predicted models was considered for further analysis (Supplementary Table 2).

Next, we performed all atom MD simulation in aqueous environment to assess the interaction stability of the STX11 H_{abc} and Orai1 C-terminus complex. The STX11 H_{abc} remained conformationally stable throughout the simulation time as assessed through RMSD (Supplementary Figure 8). The binding energy (Supplementary Figure 9) and the interaction between the two subunits remained largely stable throughout the simulation period (Movies 1-3). Major interactions observed include salt bridge between Arg78_STX11 and Glu275_Orai1, Glu150_STX11 and Arg289_Orai1, Arg160_STX11 and Glu272_Orai1, H-bond between Asn147_STX11 and Arg289_Orai1 and Gln164_STX11 and Glu272_Orai1. A potential cation-pi interaction between Tyr146_STX11 and Arg289-Orai1 was also observed in one of the replicates (Supplementary Figure 10).

The individual trajectories were concatenated and clustered to obtain a centroid structure for this complex. There were 46 clusters, and the largest cluster had 52 members. The cluster representative of the largest cluster showed the elaborate protein-protein interface, and the Orai1 C-terminus was found to be oriented in an anti-parallel orientation to the STX11 H_{abc} (Figure 3H, 3I) and we observed 4 salt bridge and 13 H-bond interactions (Figure 3J). Overall, the docking and simulation analysis corroborated the biochemical findings and demonstrated a direct role of STX11 in the regulation of Orai1.

Upon store depletion Stim is known to localize to ER-PM junctional regions where it traps and co-clusters with Orai1. To further understand the mechanism of action of STX11 in SOCE, we first assessed whether the localization of Orai and Stim was normal in control and STX11 depleted cells. We imaged HEK293 cells expressing CFP-Orai1, Stim1-YFP under resting or store depleted conditions, comparing the levels of Orai1, Stim1 in the PM or in ER-PM junctions (also termed puncta) across control or STX11 depleted cells. Although the distribution of resting and store-depleted Stim1-YFP appeared normal (Figure 4A, 4B), CFP-Orai1 appeared partly diffuse in STX11 deficient store-depleted cells (Figure 4B). Because Stim clusters Orai, we first quantified Stim1-YFP intensity within ER-PM puncta of store-depleted HEK293 cells. We found no defect in the ability of Stim1 to localize and cluster in the ER-PM junctions upon store-depletion (Figure 4C). In line with these findings, measurement of the ER calcium content by stimulating control and STX11 depleted cells with Ionomycin showed no significant change (Supplementary Figure 11) and staining of ER and Golgi with organelle specific markers also showed no abnormalities (Supplementary Figures 12A and 12B) suggesting that the overall health and calcium content of ER and Golgi were not adversely affected by STX11 depletion. However, quantification of Orai1 intensity revealed that the fraction of Orai1 inside Stim:Orai puncta showed a consistent decrease (Figure 4D) while fraction of Orai1 outside puncta was found to be higher (Figure 4E). To assess whether the level of Orai1 expression in the plasma membrane was normal, we labelled a U2OS cell line stably expressing Orai1 tagged with a Bungarotoxin binding site (BBS) in the second extracellular loop and YFP at C-terminus (Orai-BBS-YFP) with Alexa-647 conjugated

bungarotoxin (BTX-A647) (Supplementary Figures 13) [16]. We found no change in the expression levels of total Orai1 in the PM of STX11 depleted cells (Figure 4F). Large fluorescent tags can sometimes cause steric hindrance in certain locations. Therefore, we reversed the direction of fluorescent tags on Orai1 as well as Stim1 and repeated the experiment described above. Expression of Orai1-CFP and YFP-Stim1 could overcome the apparent defect in the entrapment of Orai by Stim in STX11 depleted HEK293 cells (Figure 4G-J). However, SOCE was still significantly inhibited in Orai1-CFP and YFP-Stim1 expressing HEK293 cells (Figure 4K). These data demonstrate that STX11 binding to resting Orai1 has implications beyond mere co-entrapment of Stim1 and Orai1. Collectively, these data suggest that STX11 regulates functional entrapment as well as subsequent gating of Orai by Stim.

To further establish that STX11 depletion mediated suppression of SOCE encompasses a defect in Orai gating, we expressed Orai1 tethered to two Stim-Orai activating regions (SOAR) of Stim1 [38] and eGFP (Orai1-S-S-GFP) (Supplementary Figure 14) in HEK293 cells. Orai1-S-S-GFP has previously been shown to constitutively activate Orai1 [39]. We found that in STX11-depleted, Orai1-S-S-GFP expressing cells, constitutive calcium entry was significantly smaller in magnitude (Figure 5A-B). To determine whether reduced calcium entry resulted from a defect in the ability of SOAR to independently bind Orai1, we next expressed YFP-tagged soluble CRAC activation domain (CAD) of Stim1, YFP-CAD, in Orai1-CFP expressing stable HEK293 cell line. YFP-CAD localizes to the cytosol in HEK293 cells but in cells overexpressing Orai1, a significant majority of it localizes to the plasma membrane due to its association with Orai1 [40]. We quantified the amount of YFP-CAD localized to the PM as a fraction of total YFP-CAD expressed in each cell and found no defect in its ability to localize to the plasma membrane in STX11 depleted Orai1-CFP expressing cells (Figure 5C-D). However, in line with our observations with Orai1-S-S-GFP, constitutive calcium entry was significantly reduced (Figure 5E-G). Finally, we expressed the constitutively active H134S mutant of Orai1 in HEK293 cells and measured calcium influx. H134S Orai1 harbors an open pore and the C-terminal cytosolic tails of Orai1 are unlatched, straightened and pointing towards the cytosol [41, 42]. Remarkably, expression of H134S Orai1 completely restored constitutive

339 calcium influx in STX11 depleted cells (Figure 5H, 5I). Taken together, these data suggest
340 that by binding to the resting Orai1 cytosolic tails, STX11 facilitates a structural transition,
341 such as correct alignment of Orai1 C-termini, which prepares Orai for gating by Stim.
342 Therefore, our studies have unraveled a SNARE dependent priming step in the process
343 of Orai1 gating, which cannot be compensated by merely increasing the density of Stim
344 proteins bound to Orai.
345
346 Human patients with mutations in STX11 develop a rare but fatal autoimmune
347 disease known as familial hemophagocytic lymphohistiocytosis type 4 (FHLH4) [43]. The
348 primary cause of this life-threatening disease is a defect in the cytolytic activity of T
349 lymphocytes and NK cells, which renders the patients susceptible to recurrent infections.
350 Patients suffer from high fever and severe lymphopenia in early infancy and succumb to
351 the disease by adolescence unless given bone marrow transplants. Given that STX11
352 deficient T cells exhibit a strong defect in SOCE which is known to be crucial for
353 degranulation [3] [4] [5], we hypothesized that reduced SOCE is the primary cause of
354 cytotoxicity defects in FHL4 patient T cells. To test our hypothesis, we isolated PBMCs
355 from a 4 year old FHLH4 patient with a homozygous deletion frameshift mutation in the
356 STX11 coding sequence, c.752delA:p.Lys251fs. The patient presented with typical
357 symptoms of FHLH4 disease. Given the limited amount of sample available from the
358 patient, we periodically stimulated patient and healthy donor PBMCs with PHA and
359 cultured them in IL-2 to expand their numbers, prior to analysis *in vitro*. Isolation and
360 Sanger sequencing of the patient PBMC DNA showed deletion of a single Adenine at the
361 752nd position in the STX11 gene (Figure 6A), which would lead to frameshift as well as
362 elongation of the transcript, resulting in altered protein sequence following Lysine 251.
363 Supplementary Figure 15 shows the schematic of the wildtype and predicted mutant
364 STX11 proteins, with the estimated molecular weight of mutant STX11 predicted to be
365 39.5 KDa. To determine whether the elongated mutant STX11 protein was expressed,
366 whole cell lysates prepared from the FHLH4 patient and healthy donor PBMCs were
367 subjected to SDS-PAGE and Western Blot. While the wildtype STX11 band (~33 KDa)
368 was absent in the patient lysate, we observed a faint but distinct band running higher, at
369 around 37 KDa, in the FHLH4 sample (Figure 6B). Therefore, the observed and predicted

molecular weight of the FHLH4 mutant protein was higher but its expression was significantly reduced compared to the wildtype STX11 likely due to protein instability and degradation. In accordance with our findings in the STX11 depleted Jurkat T cells, SOCE was found to be significantly defective in the FHLH4 patient T cells when compared to healthy donor T cells (Figure 6C). Further, expression of wildtype STX11 in FHLH4 T cells reversed the SOCE defect (Figure 6D), conclusively ruling out any additional abnormalities in patient T cells and like in the case of Jurkat and HEK293 cells (Figure 1H and Supplementary Figure 4), expression of STX11 in wildtype PBMCs resulted in a significant increase in SOCE (Figure 6E-F). We next performed granule release assay on the *in vitro* cultured control and FHLH4 patient CD8 T cells in response to receptor (anti-CD3+anti-CD28) mediated stimulation (Figure 6G, 6H). We observed a ~50% defect in the FHLH4 patient CD8 T cell degranulation. To determine whether the reduced granule release results from a direct defect in vesicle fusion or SOCE, we stimulated the cells with Ionomycin+PMA (Figure 6G, 6H). Remarkably, cytolytic activity was fully restored in FHLH4 patient T cells demonstrating that defective SOCE largely causes the cytolytic defects in FHLH4 patient T cells. Further, we stimulated WT and FHLH4 PBMCs either through the receptor (anti-CD3+anti-CD28) or using Ionomycin+PMA, extracted total RNA and performed Q-PCR to assess Interleukin-2 (IL-2) expression. As seen previously with Jurkat T cells (Figure 2), IL-2 expression was significantly defective in FHLH4 patient T cells but could be largely restored with Ionomycin (Figure 6I). Taken together, these data show that reduced SOCE primarily causes the cytotoxicity and gene expression defects in FHLH4 patient T cells resulting in immune dysregulation. These defects likely together initiate the pathogenesis of the complex FHLH4 disease in human patients.

Finally, Q-SNAREs, such as syntaxins, are often found in complex with other Q-SNAREs such as SNAP23/25/29 in the target membranes. A number of previous studies have implicated the complex of SNAP23/25 and STX1a in the regulation of a variety of ion channels [26, 29]. The three SNAPs, SNAP23/SNAP25/SNAP29 are each capable of contributing two SNARE domains to the *trans*- and *cis*-SNARE complex although they themselves lack a transmembrane domain and are attached to the target membrane *via* palmitoylation of specific residues. Depletion of SNAP23/SNAP25/SNAP29 did not show

a significant reduction in SOCE (Supplementary Figure 1E-1G). To determine whether SNAP23/SNAP25/SNAP29 might still form a part of the STX11:Orai complex to regulate SOCE, we co-expressed flag-tagged Orai with myc-tagged respective SNAPs and performed co-immunoprecipitations. We did not find any interaction between the three SNAPs and Orai1 (Supplementary Figure 16). Similar studies were performed by co-expressing YFP-Stim1 and the respective SNAPs. Again, no interaction was found between the three SNAPs and Stim1 (Supplementary Figure 17). These data show that, unlike in the case of *trans*- and *cis*-SNARE complexes, STX11 does not collaborate with SNAP23/SNAP25/SNAP29 in the regulation of SOCE. Figure 7 proposes a model to summarize the interaction of Orai1 with STX11 which is necessary for and precedes store-operated gating of Orai1 channels.

Discussion:

CRAC channels conduct a small but highly calcium specific current in response to store-depletion. According to the prevailing view, Orai proteins, which reside in the plasma membrane, depend on the ER resident store sensor Stims for the structural transitions leading up to their activation[7]. Unlike other ion channels, the process of activation of CRAC currents is exceptionally slow. For instance, following break-in or store-depletion, it takes, on average, ~5 minutes for Stims to cluster in the ER-PM junctions and for measurable CRAC currents to flow. It is believed that during this time, all the action happens at the level of Stim proteins, which undergo intramolecular transitions and slowly trap and gate freely diffusing Orai. This makes Orai proteins a completely passive player in SOCE.

We have shown that the cytosolic tails of Orai1 constitutively couple with STX11 in resting cells (Figure 3). Interestingly, Orai cytosolic tails have been shown to be crucial for gating but are missing from the structures of closed and open *Drosophila* Orai [41, 44]. The structure of closed Orai suggested that C-terminal tails of two adjacent Orai subunits, bend, pair with each other in an antiparallel fashion and sit closely apposed to the plasma membrane. However, in the structures of the constitutively active H134 mutant Orai, the C-terminal tails are found to orient away from the plasma membrane [41, 44]. Unlike wildtype Orai1, the H134S Orai1 mutant was insensitive to STX11 depletion. Therefore, it is reasonable to propose that STX11 binding to resting Orai1 facilitates a structural transition which enables Stim dependent gating of Orai in ER-PM junctions. Such molecular transition should logically precede the association of Orai with Stims because the STX11 and Stim1 interacting regions appear to be overlapping in Orai1. Of note, STX11 did not co-localize with Orai and Stim in ER-PM junctions (Supplementary Figure 18). In line with those findings, STX11 also did not appreciably co-immunoprecipiate with Stim1 (Supplementary Figure 19). Therefore, our data suggest that STX11 comes off Orai after having induced the proposed structural change. In a different scenario, change in either the structure of STX11 itself or antibody accessibility/ affinity could have precluded detection of STX11 in Stim:Orai clusters.

FHLH is a heterogeneous autoimmune disorder where patients suffer from hyperinflammation and severe dysregulation of the immune system. Defects in the CTL and NK cell cytotoxicity machinery underlie the development of this complex disease. Several genes such as *STX11*, *UNC13D*, *Prf1*, *Rab27*, *Munc18-2* and sometimes *XIAP* and *ITK* are broadly grouped together based on disease symptoms, although the age of onset and severity varies across the spectrum [45 46 47]. Most mutations in the *STX11* coding region result in a complete loss or a severe depletion of the protein levels [48]. The disease, therefore, results from reduced STX11 protein in most FHLH4 patients. Of note, we saw a ~50% defect in CTL degranulation and a ~70% defect in IL-2 expression even though the patient exhibited all the typical symptoms of FHLH4 by 4 years of age. A partial defect in degranulation is not surprising given that *in vitro* culture of FHLH patient CTLs in the presence of IL-2 has been previously shown to overcome the cytolytic defect [49]. In those studies, IL-2 dependent induction and compensation by STX3 was proposed to cause the reversal of the granule release defect *in vitro* [49]. Therefore, it is likely that an analogous mechanism partially rescued the degranulation defect in the *in vitro* cultured FHLH4 patient PBMCs in our study. Another possibility is that the residual STX11 mutant protein retained function in FHLH4 T lymphocytes (Figure 6B). Nevertheless, in addition to the cytolytic defects, for the first time, we have shown that STX11 deficient T cells harbor a severe defect in SOCE, downstream signaling and gene expression. Therefore, STX11 deficiency affects T cell activation and FHLH4 disease progression at multiple levels. We propose that the design and early administration of CRAC channel agonists could potentially provide an alternative to bone marrow transplants for FHLH4 patients.

In summary, we have shown that binding to a Q-SNARE, STX11, provides an on-site molecular switch necessary for a previously unsuspected crucial priming of the CRAC channel pore, Orai. This, SNARE enabled, structural transition is necessary for the gating of CRAC channels. We argue that ion channel regulation is a novel, direct and primary role of specific Q-SNAREs, such as STX11. In accordance with this hypothesis, SNAREs are now thought to have evolved from a common archaeal precursor found to be present in the genomes of Asgard and members of *Legionella* [50]. Both organisms lack an endomembrane system but do express ion channels and transporters.

Materials and Methods

Plasmid constructs and transfection

Orai1-Myc, Flag-Orai1, Stim1-Myc, Orai1-CFP, Orai1-YFP, CFP-Orai1, YFP-Orai1, YFP-Stim1, Orai-BBS-YFP, Orai1-S-S-EGFP, CFP-Stim1, Stim1-CFP, YFP-Stim1 and Stim1-YFP plasmids have been described previously [17] [19]. Stim1 CAD was sub-cloned in eYFPC1 vector after amplification from YFP-Stim1 plasmid to generate YFP-CAD. pLKO.1, psPAX2 and pMD2.G were purchased from Addgene. pLKO.1 cloned shRNA sequences targeting the genes of interest, were either purchased from Horizon Discovery, UK or designed and cloned in-house using the Broad Institute portal (https://portals.broadinstitute.org/gpp/public/gene/search). Full-length human STX11 was cloned from human cDNA prepared from HEK293 cells and subcloned into pcDNA3.1(+), pcDNA/4TO/Myc-HisA (Invitrogen, Grand Island, NY), pMSCV-IRES-mcherry (Addgene), pEF1alpha-IRES (Clontech) and pET28b vector [19] with an N-terminal 6XHis-tag. The fragments of STX11 were cloned in pET28b vector with an N-terminal 6xHis tag for expression in *E. Coli*. HA tag was inserted between H30 and G31 in Stx11 cloned in pMSCV-IRES-mCherry construct using PCR. Point mutants of Orai1 (H134S) were generated using site directed mutagenesis. The fragments of Orai1 (1-87, 1-47, 48-103, 256-301 and 272-292) were amplified from full length constructs and cloned into pMAL-c5X vector (New England Biolabs), in-frame with MBP protein coding sequence, as described previously [19]. SNAP23, SNAP25 and SNAP29 cDNA cloned in pCMV-Sport6.1 vectors were purchased from Dharmacon and subcloned into pcDNA4/TOMycHisA. SNAP23 was subcloned in pMAL-c5X vector in-frame with MBP. All plasmid DNA transfections in human cell lines and primary cells were done using Lipofectamine 2000 (Invitrogen)/ Lipofectamine 3000 (Invitrogen) or Amaxa nucleofection kit (Lonza, Basel, Switzerland) respectively, as per manufacturer's protocol.

Cell Lines

Lentiviral shRNA transduction experiments were performed in HEK 293, U2OS or Jurkat (ATCC, Manassas, VA) cell lines cultured in low glucose DMEM (Hyclone, Logan, UT) or RPMI (Hyclone) respectively, with 5-10% fetal bovine serum (Hyclone), 1X Penicillin

Streptomycin, and GlutaMax (Gibco, Grand Island, NY). Stable cell lines generated using HEK293 and U2OS parent lines have been described previously [16]. HEK293-FT cell line was cultured in high glucose DMEM with 10% FBS and 10mM HEPES, 1X Penicillin Streptomycin, 1X GlutaMax and 1X non-essential amino acid and transfected with the appropriate plasmids to generate viral supernatants. All cell lines were tested for mycoplasma contamination twice every year, and found to be negative.

Antibodies and Reagents

Antibodies/Reagents	**Source and Cat no**	**Dilution/ Conc.**
Mouse anti-myc (9E10)	Abcam #ab32	1:1000
Mouse anti-myc (9E10)	Culture supernatant, in house	1:1000
Rabbit anti-SNAP23	SYSY#111203	1:1500
Mouse anti-SNAP25	SYSY#111011	1:1500
Rabbit anti-SNAP29	SYSY#111303	1:1500
Rabbit anti-GFP	Invitrogen#A11122	1:2500
Rabbit anti-flag	Sigma#F7425	1:1600
Mouse anti-flag (M2)	Sigma#F3165	1:1500
Mouse anti-6X His	Invitrogen #MA1-135	1:2000
Rabbit anti-Stx11	Sigma#SAB4301593	1:1000
Mouse anti-NFATc2 (4G6-G5)	Santacruz#7296	1:500
Goat anti-Lamin B (M-20)	Santacruz#6217	1:500
Rabbit monoclonal anti-HA	CST#3724S	1:1000
Alpaca VHH anti-rabbit AF488	Jackson #611-544-152	1:400 (1.375μg/ml)
DAPI	Invitrogen #D1306	2μg/ml
Rabbit anti-Stx11	SySy #110113	1.67μg/ml
Rabbit anti-Stx11	Invitrogen #PA5-50800	1:2000

Goat anti-rabbit A647	Invitrogen #A-21245	1:800
Rabbit anti-Stx11	Proteintech #13301-1-AP	0.3μg/ml
Donkey anti-rabbit A647	Jackson #711-605-152	1:800
HRP GAPDH	Sigma #G9295	1:40000
HRP Donkey anti-Rabbit	Jackson #711-035-152	1:50000
HRP Donkey anti-Mouse	Jackson #715-035-151	1:50000
Rabbit anti-NFAT1	Cell Signaling Technology	1:200
Ultra-LEAF Purified anti-human CD3	Biolegend #317326	5-10μg/ml
Ultra-LEAF Purified anti-human CD28	Biolegend #302934	2μg/ml
Ultra-LEAF Purified anti-human CD49d	Biolegend #304340	2μg/ml
PE anti-human CD107a (LAMP-1)	Biolegend #328608	1:50
APC anti-human CD8 antibody	Biolegend #344722	0.5μg/ml
Fura-2-AM	Invitrogen #F1221	1μM
Thapsigargin (TG)	Sigma #T9033-1MG	1μM
Polybrene (Hexadimethrine-bromide)	Sigma #107689-10G	8μg/ml
NE-PER kit	Thermo #78833	
Protein A/G Mag Sepharose xtra	Cytiva #28967056/66	
Protein A/G 4 Fast Flow Sepharose	Cytiva #17528001	
Protease Inhibitor Cocktail (Mammalian)	Sigma #539134	
Protease Inhibitor Cocktail (Bacterial)	Calbiochem #539132	
Talon Beads	Takara #635502	
Dextrin Sepharose Beads	Cytiva #28935597	
HEPES	Sigma #H3375-100G	
Lipofectamine 2000	Thermofisher #11668019	
Lipofectamine 3000	Thermofisher #L3000001	
Lemo21(DE3) *E.coli.* cells	NEB #C2528J	
IPTG	Himedia #MB072-10G Sigma #16758-10G	
Sarkosyl (N-lauroylsarcosine sodium	Sigma #L9150-50G	

salt)		
Lysozyme	Sigma #62970-5G-F	
DNaseI Recombinant RNase-free	Roche #04716728001	
PMA (Phorbol Myristate Acetate)	Sigma #P8139	20-50ng/ml
Ionomycin	Sigma #407952	1μM
Human IL-2 protein	Acro Biosystems #H5215	50ng/ml
Lectin from *Phaseolus vulgaris* (PHA)	Sigma #L8754	2μg/ml
Retronectin	Takara #T100B	20μg/ml
RNeasy Plus Mini kit	Qiagen#74134	
QIAshredder	Qiagen#79654	
Superscript IV	ThermoFisher#18091300	
Qubit ssDNA Assay kit	ThermoFisher# Q10212	
Human Stx11 TaqMan probe (FAM-MGB)	ThermoFisher# Hs00186823_m1	
Human Beta Actin TaqMan probe(FAM-MGB)	ThermoFisher# Hs01060665_g1	
Human IL2 Taqman probe (FAM-MGB)	ThermoFisher# Hs00174114_m1	
Paraformaldehyde	Electron Microscopy Sciences #157-8	
Bovine Serum Albumin	Jackson #001000173	
Luria Bertini Broth	Himedia #M1245	
HBSS	Sigma #H8264	
Terrific Broth	Sigma #T9179	
Alexa fluor 647 conjugated Alpha Bungarotoxin	Invitrogen #B35450	1μg/ml
HRP rabbit anti-GFP	Invitrogen #A10260	
HRP Goat anti-rabbit Fc	Jackson #111-035-008	1:50,000
Ampicillin	Sigma #A0166-5G	
30% Acrylamide:Bis Solution (29:1)	Biorad #1610156	

DTT (Dithiothreitol)	Biorad #1610611	
0.05% Trypsin-EDTA	Gibco #25300054	
100X Penicillin Streptomycin	Sigma #P4333-100ML	
Puromycin	Gibco #A11138-03	
Pluronic F-127 (20% solution in DMSO)	Invitrogen #P3000MP	0.02%

Lentiviral transductions

For the generation of lentiviral supernatants, shRNAs cloned in pLKO.1 were co-transfected with psPAX2 packaging plasmid and pMD2.G envelope plasmid into HEK293-FT cells using the calcium phosphate method of transfection. 48 and 72 hours post-transfection, viral supernatants were collected, pooled and stored at -80°C till further use. For transduction of HEK293 and Jurkat cells, 0.1 million cells were plated in 6- or 24-well plates either the day before (HEK293) or the same day (Jurkat). Viral supernatants were added to the cells along with 8ug/ml polybrene and cells were spun at 2500 RPM, 30°C for 90 mins. 24 hours or 48 hours post-spinfection, Puromycin was added at a final concentration of 1ug/ml to HEK293 and Jurkat cells, respectively. Cells were analyzed 3-5 days post transduction.

Immunocytochemistry and confocal imaging

For Stx11 localization, resting or store-depleted (1μM Thapsigargin) WT HEK293 or HEK293 cells stably expressing Orai1-YFP were either plated in 6 well plates and spinfected with viral supernatants generated from pMSCV-Stx11(HA)-IRES-mCherry, pMSCV-IRES-mCherry (empty vector control) or plated in carbon coated, glow discharged 35mm glass bottom dishes (IBDI) and transfected with pEF1alpha-Stx11-IRES-mCherry. 24 hr post-spinfection, cells were plated in 35mm glass bottom dishes. For immunolabelling, cells were washed with Ringer's buffer, fixed with 4% PFA and blocked with 3% BSA containing 0.1% NP40 for 1.5 hrs. Post-fixation and permeabilization, cells were incubated either with anti-HA (CST) or rabbit anti-Stx11 (SySy/ Proteintech) primary antibodies O/N at 4°C, washed and incubated with either Alpaca VHH anti-rabbit AF488, donkey anti-rabbit A647 or goat anti-rabbit A647

559 secondary antibodies for 1 hour at room temperature (RT). Cells were counter stained
560 with DAPI for 10 min at RT and imaged using Olympus FV3000 laser scanning
561 microscope. Images were acquired sequentially using the following parameters: DAPI
562 (DM405/488 dichroic, 405nm excitation, 430-470nm emission); anti-HA Alexa488
563 (DM405/488, 488nm excitation, 500-590nm emission); Stx11 (DM405/488/561/640,
564 640nm excitation, 650-750nm emission); Orai1-YFP (DM405/488/561/640, 488nm
565 excitation, 521-591nm emission); CFP-Stim1 (DM405-445/514/594, 405nm excitation,
566 448-510nm emission).
567
568 **Quantification of Orai1 and Stim1 intensities inside/outside ER-PM puncta**
569 HEK293 cells were plated in 6 well plates and transduced with scramble or STX11
570 shRNA. 48hr post transduction, cells were trypsinized and plated in carbon coated 35mm
571 dishes and co-transfected with CFP-Orai1 and Stim1-YFP. Images were acquired
572 sequentially for CFP and YFP using Olympus FV3000, using 405nm and 514nm lasers
573 respectively using a 60X objective. Cells were washed and incubated in Ringer's buffer
574 prior to imaging and the positions of CFP and YFP double positive cells were marked.
575 Resting Orai1 and Stim1 images were acquired first. Following this, cells were incubated
576 with Thapsigargin (1uM) plus EGTA (10mM) for ~8 mins before capturing the store-
577 depleted images. The imaging was done in live cell chamber to maintain the temperature
578 at 37C. For analysis, Stim1-YFP images were masked using Phansalkar local
579 thresholding in ImageJ software. Stim puncta were detected on the image mask using
580 "Analyze Particles" in ImageJ and used for determining the intensity values of CFP-Orai1
581 and Stim1-YFP inside Stim1:Orai1 co-clusters. Cell boundaries were manually drawn
582 using CFP-Orai1 images and total Orai1 intensities were obtained using these ROIs. The
583 Stim/ Orai intensity values obtained from the above analysis were plotted using Origin
584 software. In the experiment where the direction of fluorescent tags on Orai1 and Stim1
585 were flipped, Orai1-YFP or CFP-Stim1 expressing cells were transduced with scramble
586 or STX11 shRNA and plated as mentioned above. Images were acquired using a TIRF
587 microscope setup described before [14]. Images were captured in resting cells and positions
588 marked. Store-depleted images were acquired after incubation with 1uM Thapsigargin
589 (TG) and 10mM EGTA for ~6 mins. Analysis was done as mentioned above with Otsu

local thresholding in ImageJ software. Stim1 and Orai1 intensity (AU) and area (pixels) values obtained from the analysis were plotted using Origin software.

Alpha-bungarotoxin binding assay

U2OS cell line stably expressing Orai1-BBS-YFP construct has been described previously[14]. Briefly, Orai1-BBS-YFP expressing U2OS cells were transduced with scramble or Stx11 shRNA. Cells were trypsinized 3-4 days post-transduction, centrifuged and labelled on ice with AF647 conjugated alpha-bungarotoxin (1μg/ml) containing 2% FBS in 1X HBSS for 30 mins. Following this, cells were washed with HBSS and fixed with 4% PFA (~20 min at RT). Samples were run using Cytoflex FACS analyzer (Beckman Coulter) and data were analyzed using Flow Jo software.

Validation of Stx11 knockdown using QPCR

Scramble and Stx11 shRNA treated HEK293 cells were trypsinized, counted and equal number of cells were used for lysis. The lysates were homogenized using QIA shredder columns (Qiagen) and RNA isolation was done using RNeasy Plus Mini kit (Qiagen). Total RNA isolated from both the groups was used for cDNA synthesis using oligo dT primers and Superscript IV as per manufacturer's guidelines. The concentration of synthesized cDNA was estimated using Qubit ssDNA assay kit and STX11 TaqMan probes were used to perform the QPCR using LightCycler 96 (Roche). Beta-actin was used as housekeeping control.

Single cell Ca^{2+} imaging

Cells were plated in carbon-coated glass bottom dishes (one day prior or 30 mins before the assay for HEK293 and Jurkat T cells respectively) and loaded with 1uM Fura-2 AM dye in HBSS ($CaCl_2$ 1.8mM, KCl 5.36mM, $MgSO_4$ 0.81mM, NaCl 136.89 mM, Na_2HPO4 0.335mM, D-Glucose 5.55mM) for 30 mins, at 37°C in the dark. After incubation, cells were washed and incubated in Ringer's buffer (135mM NaCl, 5mM KCl, 1.8mM $CaCl_2$, 1mM $MgCl_2$, 5.6mM Glucose, 10mM HEPES) for an additional 10 mins, washed and imaged in Ringer's buffer or Calcium-free Ringer's buffer (135mM NaCl, 5mM KCl, 1mM $MgCl_2$, 5.6mM Glucose, 10mM HEPES at pH7.5), as indicated. Olympus IX-71 inverted

621 microscope equipped with a Lamda-LS illuminator (Sutter Instrument, Novato, CA), Fura-
622 2 (340/380) filter set (Chroma, Bellows Falls, VT), a 10X 0.3NA objective lens (Olympus,
623 UPLFLN, Japan), and a Photometrics Coolsnap HQ2 CCD camera was used to capture
624 images at a frequency of ~1 image pair every 2 or 4 seconds interval. Approximately 30-
625 50 cells were imaged per group in each experiment unless otherwise stated. Data were
626 acquired, analyzed and plotted using MetaFluor (Molecular Devices, Sunnyvale, CA),
627 Microsoft Excel, and Origin softwares.
628 For constitutive calcium influx assay, shRNA treated HEK293 cells were either
629 transfected or nucleofected with Orai1-S-S-EGFP or Orai1(H134S)-YFP and ~12-14 hour
630 post transfection (~4-5 hour post nucleofection), cells were loaded with Fura-2 AM,
631 washed and imaged in Ringer's buffer with 0mM calcium to acquire baselines and 2mM
632 calcium thereafter. To measure CAD induced constitutive calcium influx, Orai1-CFP
633 expressing stable HEK293 cells were nucleofected with YFP-CAD and analyzed ~4 hour
634 later as described above. To identify cells expressing Orai1 mutants and fusion proteins
635 in the plasma membrane, cells were imaged using a 20X 0.7NA water objective lens
636 (Olympus, UApoN340, Japan). Images were acquired at a frequency of ~1 image pair
637 every 10 seconds interval to avoid photobleaching and analyzed as described above.
638
639 **Measurement of NFAT nuclear localization by Western Blot**
640 Jurkat T cells were transduced with scramble or STX11 shRNA to knock-down STX11 as
641 described above. On day 4 post-transduction, cells were collected, spun down and
642 resuspended in plain RPMI media and rested for 1hr at 37°C. Following this, cells were
643 counted and divided into two equal groups. One group was resuspended in RPMI
644 (unstimulated) and the other in RPMI media containing 1uM TG + 10ng/ l PMA (Phorbol
645 Myristate Acetate) (stimulated) and incubated at 37°C for 30 mins. Following incubation,
646 cells were pelleted and the nuclear and cytosolic protein fractions were separated using
647 NE-PER kit according to the manufacturer's guidelines and subjected to SDS-PAGE and
648 Western Blot using the mouse anti-NFATc2 primary antibody (Santa Cruz) followed by
649 Donkey anti-mouse secondary antibody.
650
651 **Estimation of nuclear translocation of NFAT in Jurkat T cells by imaging**

Control and STX11 depleted Jurkat T cells were rested in plain RPMI for ~1 hour prior to the assay. ~100,000 cells per group were plated on freshly carbon-coated coverslips for 40 minutes and stimulated for 1 hour at 37°C with 5 ug/ml anti-CD3 antibody, diluted in plain RPMI. Following this, cells were washed and fixed using 4% PFA diluted in 1X PBS for 20 minutes at RT, washed twice and incubated with 30 mM Glycine for 10 minutes at RT. For permeabilization and blocking, cells were incubated with 0.1% Saponin, 3% BSA diluted in 1X PBS for 1 hour at RT, washed and incubated with anti-NFAT primary antibody (anti-NFAT1, CST) at 4°C, overnight. Following primary antibody application, cells were washed with 1X PBS and incubated with anti-Rabbit AF647 secondary antibody for 1 hour, washed and stained with DAPI for 5 minutes followed by additional washes. Images were acquired in the FV3000 confocal microscope. DAPI was used to identify the nuclear area. Nuclear *versus* whole cell (total) NFAT mean intensity ratio was plotted across different groups.

Whole cell lysates (WCLs), Western Blot and Co-immunoprecipitation (Co-IP)

HEK293 cells transfected with the desired plasmids were lysed using buffer containing 50mM Tris-Cl (pH 8.0), 150mM NaCl, 1% NP-40, 1mM PMSF, and protease inhibitor cocktail. The whole cell lysates were centrifuged at 21000g for 15 minutes and supernatants were subjected to SDS-PAGE, and Western Blot. For immunoprecipitations, lysates were divided into two equal parts. To the first tube, the appropriate anti-mouse or anti-rabbit primary antibody was added and to the second, same amount of the respective IgG control antibody was added. The antibody-lysate mixtures were incubated overnight at 4°C. Following this, Protein A/G Mag Sepharose beads were added and incubated with the antibody-lysate mixtures for 4 hours, washed with the lysis buffer containing 0.1% NP-40, boiled with 1X Laemmli buffer + 120mM DTT and subjected to SDS-PAGE and Western Blot analysis. Typically, 1/10th of the whole cell lysate (WCL) was loaded in the input lane of the co-IP blots.

***E. coli* expression and *in-vitro* binding assays**

Full-length His_6-tagged Stx11 and truncation mutants were cloned in pET28b, expressed in Lemo21 (DE3) *E. coli* cells and induced with 1mM IPTG (Isopropyl β- d-1-thiogalactopyranoside) for 14-18 hours at 18°C. The cell pellets were lysed in buffer containing 50mM Tris-Cl (pH 8.0), 150mM NaCl, 10% Glycerol, 1mM PMSF, 1% Sarkosyl, 0.1mg/ml Lysozyme, protease inhibitor cocktail and sonicated on ice. DNase I was added after sonication and the lysates were further incubated for ~60 minutes before centrifugation at 21000g for 40 mins. The supernatants were subjected to SDS-PAGE to confirm expression by Coomassie staining and subsequently used for pull-down assays. MBP-tagged Orai1 constructs were expressed in Lemo21 (DE3) *E. coli* cells, induced with 0.3mM IPTG (Isopropyl β- d-1-thiogalactopyranoside) for 14-18 hours at 18°C. The cell pellets were lysed in buffer containing 50mM Tris-Cl (pH 8.0), 150mM NaCl, 5% Glycerol, 1mM PMSF, 0.1mg/mL Lysozyme and protease inhibitor cocktail (1:200) and sonicated on ice. DNase I was added after sonication and the lysates were further incubated for ~60 minutes before centrifugation at 21000g for 40 mins. The supernatants were collected and subjected to SDS-PAGE to confirm expression by Coomassie staining and used for pull-down assays. Following lysis, the His_6-tagged Stx11 proteins were purified using Talon Beads and MBP-tagged Orai1 proteins using Dextrin Sepharose/Amylose resin according to the manufacturer's guidelines. For *in-vitro* binding assays, lysates prepared from cells expressing MBP or MBP-tagged Orai1 fragments were incubated with 25μL Dextrin Sepharose Beads and incubated for 2 hours at 4°C. After incubation, beads were washed thrice and ~50-125ng of purified His-tagged full length Stx11, His-tagged SNARE or His-tagged H_{abc} domains were diluted in buffer containing 50mM Tris-Cl (pH8), 150mM NaCl, 5% Glycerol and 0.1% NP-40 and added to the beads. Following 1 hour of incubation at 4°C, the beads were washed thrice, re-suspended and boiled in the binding buffer containing 1X Laemmli and 120mM DTT. The eluate was subjected to SDS-PAGE and Western blot. MBP and MBP-tagged proteins were detected with Ponceau staining, Full length STX11 using Rabbit anti-STX11 primary antibody (Thermo) followed by Donkey anti-rabbit HRP and His-tagged STX11 fragments were detected or mouse anti-6XHis primary antibody (Invitrogen) followed by Donkey anti-mouse HRP secondary antibody. $1/5^{th}$ of the protein was loaded in the input lane for all *in vitro* binding assays.

QPCR to estimate gene expression in Jurkat T cells

Scramble (scr) and STX11 shRNA treated Jurkat T cells were rested for ~1 hour prior to the assay, stimulated with soluble anti-CD3 (5-10 μg/ml) for 3 hours and washed with HBSS. Total RNA was isolated using RNeasy Mini kit as per manufacturer's instructions. cDNA was synthesized using random hexamers and Invitrogen Superscript IV kit and quantified using Qubit ssDNA assay. Taqman probes for IL-2 and beta-actin housekeeping control were used for performing the QPCR in triplicates. Data analysis was done by calculating the double delta C_t values.

Isolation and culture of human PBMCs

All experiments with human PBMCs were approved by the Institutional Human Ethics Committee. Healthy human whole blood freshly collected in heparin or Citrate Phosphate Dextrose Adenine (CPDA) solution was subjected to density gradient centrifugation using Ficoll-Paque PLUS media. The buffy coat was separated, washed twice with HBSS and cultured with IL-2 (50 ng/ml). Cells were stimulated once per week with PHA (2 ug/ml) for 72 hours and rested in IL-2 for the remaining 72-96 hours. Unless specified, all the assays were performed following 24-48 hours of rest, post stimulation.

Isolation of genomic DNA and sequencing of FHLH4 patient mutation.

Genomic DNA was extracted from healthy donor and FHLH-4 patient PBMCs using Phenol-Chloroform-Isoamyl alcohol. Stx11 genomic region flanking the mutation was PCR amplified using primers: 5' Forward -CATGCACGACTACAACCAGGC and 3' Reverse -GGGACAGCAGAAGCAGCAGAGGG. The resulting PCR products were separated on 2% agarose gel, excised and extracted using the Macherey-Nagel Nucleospin columns and subjected to Sanger sequencing using the 5' Forward PCR primer to confirm the mutation.

Measurement of SOCE in human PBMCs

PBMCs in culture were washed, rested and allowed to adhere to freshly carbon-coated (IBDI) dishes for 1 hour in plain RPMI at 37°C. The cells were washed with HBSS and incubated with 1ml of 1μM Fura-2-AM diluted in Ringer's buffer for 40 minutes, washed

and incubated for an additional 10 minutes to allow de-esterification of the dye. The assay was started with 1 ml of Calcium free Ringer's buffer in the imaging dish and images were captured every 4 seconds. After capturing the baseline for ~60 seconds, stores were depleted by the addition of 1 μM Thapsigargin. In other assays, 10 μg/ml of anti-CD3 and 5 μg/ml of the secondary antibody were used to cross-link the TCRs and thereby induce store depletion. ~5 minutes post-store-depletion, Calcium Chloride ($CaCl_2$) was added back to the dish at a final concentration of 2mM to estimate the magnitude of store operated calcium entry.

Degranulation assay

PBMCs were cultured in RPMI containing 10% FBS and 50 ng/ml IL-2 and stimulated with PHA (2 ug/ml) 48hrs before the assay. 24hrs prior to the assay, IL-2 was washed off but PHA was re-added. On the day of the assay cells were washed twice to remove PHA and any growth factors. To measure degranulation, cells were either left unstimulated, stimulated with a combination of anti-CD3 (10 μg/ml plate-coated), anti-CD28 (2 μg/ml soluble) and anti-CD49d (2 μg/ml soluble) or a combination of Ionomycin (1 μM) and PMA (50 ng/ml) for 3.5 hours. CD107a-PE antibody (1:50 dilution) was added to each of the three groups at the start of stimulation. Following stimulations, cells were transferred to ice, washed with cold HBSS containing 2% FBS and incubated with anti-CD8 APC for 20 minutes, washed twice with cold HBSS and analyzed using Cytoflex (Beckman Coulter) flow cytometer.

QPCR to estimate gene expression in human PBMCs

PBMCs were taken off IL-2 48 hours prior to the assay. On the day of the assay, cells were washed twice, left unstimulated and either stimulated with anti-CD3 (10 μg/ml, plate-coated), anti-CD28 (2 μg/ml) and anti-CD49d (2 μg/ml) or with Ionomycin (1 μM) and PMA (50 ng/ml) for 6 hours. To end the stimulation, cells were washed with cold HBSS, pelleted and used for RNA extraction. Total RNA was isolated using Qiagen RNeasy mini Kit and cDNA was synthesized using random hexamers and Superscript IV (Invitrogen). cDNA was quantified using Qubit and subjected to QPCR analysis using Taqman probes for IL-

2 and beta-actin housekeeping gene control in triplicates. Analysis was performed by calculating the double delta C_t values.

Transduction of human PBMCs with pMSCV-STX11

For viral transduction of PBMCs, polystyrene non-TC treated 24-well plates were coated with retronection (20 μg/ml) overnight at 4°C, blocked with 2% BSA for 30 minutes at room temperature and washed twice with HBSS. The retroviral supernatants were added onto the coated wells and the plates were spun at 1800g for 2 hours at 30°C. Following spin, the wells were washed with the blocking solution. PBMCs cultured in RPMI containing 10% FBS were stimulated with PHA (2 μg/ml) and IL-2 (50 ng/ml) for 48 hours prior to transduction. Stimulated PBMCs were transferred to coated plates at a density of 0.25 million cells/well centrifuged at 400g for 40 minutes at 30°C. The cells were analyzed 48-72 hours post transduction.

Stx11-Orai1 complex prediction

Full length STX11 and Orai1 and their two domains, (H_{abc} 41-167 and SNARE 183-267) and (N-terminus 1-87 and C-terminus 256-301), respectively were used to generate the complex of STX11 and Orai1 using AlphaFold3 (AF3) in all combinations. The resultant models were assessed using ipTM and pTM scores. The best scoring combination (STX11- H_{abc} and Orai1-C-terminus) was further considered to generate more models by changing the seed values. The best model in terms of highest ipTM and pTM values was considered for further analysis. Custom script was used to analyze the contact frequency of interacting residues of Stx11-H_{abc} and Orai1-C-terminus complex across all predicted models.

Molecular dynamics (MD) simulation

The STX11- H_{abc}-Orai1-C-terminus complex was subjected to all-atom MD simulation. Initially, the complex was prepared using protein-preparation module of Schrodinger which involves H-bond network optimization and restrained minimization of

the initial structure. The prepared structure was solvated using TIP3P water model in an orthorhombic box and neutralized by adding counter ions. OPLS4 force field was used, and simulation system was generated by specifying 150mM salt (NaCl). The solvated system was subjected to default relaxation protocol of Desmond followed by production run for 500 ns at 300K and 1 atm pressure in NPT ensemble. The default relaxation protocol includes several short simulation steps. (1) Brownian dynamics simulation for 100 ps at 10 K temperature in NVT with restraints on solute heavy atoms (2) Simulation in NVT ensemble at 10 K for 12 ps with restraints on solute heavy atoms (3) 12 ps simulation in NPT ensemble at 10 K with restraints on solute heavy atoms (4) Simulation in NPT ensemble for 12 ps with restraints on solute heavy atoms (5) Simulation in NPT ensemble for 24 ps without restraints. Three independent runs were executed with different initial seeds.

Analysis of MD simulation

The MD runs were analyzed for the stability of the complex and interactions between the subunits. The RMSD was calculated using simulation interaction diagram (SID) module of Schrodinger. The first frame was used as reference frame for RMSD calculation. Script “analyze_trajectory_ppi.py” was used to calculate the interactions between the STX11 and Orai1. The binding energy (ΔG) at each nanosecond across simulation was calculated using “thermal_mmgbsa.py” script of Schrodinger.

The representative structure was generated through trajectory clustering. The last 200 ns frames from each run were combined and clustered using scripts “trj_merge.py” and “trajectory cluster” of Schrodinger. The cluster representative of the largest cluster was used to analyze the protein-protein interactions. PDB Sum was used to calculate the interactions in the cluster representative. Figures were generated using Pymol and MD movies using Maestro.

836 **Figure Legends:-**

837

838 **Figure 1: STX11 is required for SOCE.**

839 (**A-F**) RNAi mediated depletion of STX11 reduces SOCE. Measurement of thapsigargin
840 (TG) induced SOCE in various cell lines after shRNA mediated depletion of STX11. The
841 traces in panels **A,C,E** show representative average single cell Fura-2 calcium imaging
842 assays. Bars in panels **B,D,F** show mean % SOCE ± SE from three independent
843 experiments each where mean SOCE from scramble (scr) shRNA treated group in each
844 experiment was set at 100% and the relative response of STX11 shRNA treated groups
845 was calculated respectively. **P*<0.05; ***P*<0.01; ****P*<0.001 using two-tailed Student's *t*
846 test. (**G**) Representative Fura-2 calcium imaging assay showing reconstitution of SOCE
847 in STX11 depleted Jurkat T cells by ectopic expression of STX11. Black (scr shRNA), red
848 (STX11 shRNA), green (STX11 shRNA with STX11 expression). N=2 (**H**) Ectopic
849 expression of STX11 enhances SOCE. Representative Fura-2 calcium imaging assay
850 showing SOCE in HEK293 cells expressing STX11 (red) or empty vector (EV) (black).
851 (N=3) (**I**) STX11 mediated enhancement of SOCE is dependent on Orai1. A
852 representative Fura 2 calcium imaging assay showing measurement of thapsigargin (TG)
853 induced SOCE in HEK293 cells where Orai1 expression was depleted using shRNA and
854 STX11 was over-expressed. (N=2)

855

856 **Figure 2: STX11 depletion suppresses I_{CRAC}, downstream signaling and gene**
857 **expression in Jurkat T cells.** I_{CRAC} was recorded from Jurkat T-cells in the whole-cell
858 recording configuration in 20 mM extracellular Ca^{2+} Ringer's solution. I_{CRAC} was induced
859 by passive depletion of intracellular Ca^{2+} stores by dialyzing 8 mM BAPTA into the cell via
860 the patch-pipette. (**A**) Representative current at -100 mV in Jurkat T cell transfected with
861 scr shRNA construct. The current is blocked by extracellular La^{3+} (100 µM) and replacing
862 the 20 mM Ca^{2+} Ringer's solution with a divalent free solution (DVF) evokes a large Na+
863 current which depotentiates over tens of seconds. The current-voltage (I-V) relationship
864 of the Ca^{2+} and DVF currents are shown on the right. (**B**) I_{CRAC} from a Jurkat T cell
865 transfected with STX11 shRNA. Both Ca^{2+} and Na^{+} current amplitudes are reduced
866 relative to control cells. The I-V relationships (*right plots)* show no change in ion

selectivity. (**C-D**) Summary of the current amplitudes of Ca^{2+} and Na^{+} currents and current reversal potentials in scr and STX11 knockdown cells. (**E&F**) Estimation of nuclear translocation of NFAT. (**E**) Western Blot showing nuclear translocation of NFAT in Jurkat T cells treated with scr or STX11 shRNA for 4 days and stimulated with PMA+TG for 30min prior to the preparation of nuclear and cytoplasmic extracts. (N=3) (**F**) Representative confocal images of Jurkat T cells treated with scr or STX11 shRNA for 4 days and stimulated with 10ug/ml anti-CD3 for 1 hour. Following stimulation, cells were fixed, permeabilized and stained using anti-NFAT primary antibody, followed by donkey anti-rabbit AF647 secondary antibody, and counter-stained with DAPI to mark the nuclei. (N=2) (**G**) Box and whisker plot showing percent nuclear NFAT in Jurkat T cells quantified from 40-50 cells populating 10 randomly chosen fields per group in (**F**). Boundaries of the box plots represent 25^{th} and 75^{th} percentile values, horizontal line represents mean, white circle represents median and whiskers denote the outliers. (**H**) Quantitative PCR to assess IL-2 transcription in anti-CD3 stimulated Jurkat T cells. Jurkat T cells were treated with scr or STX11 shRNA for 4 days and stimulated with 5ug/ml anti-CD3 for 3 hours. Total RNA was extracted from cells and subjected to QPCR analysis using Taqman probes for IL-2 and beta-actin. The bars show relative IL-2 mRNA expression levels with the scr shRNA treated group set at 100%. Shown here are mean ± SE. (N=3) **(F-H)** **P*<0.05; ***P*<0.01; ****P*<0.001 using two-tailed Student's *t* test.

Figure 3: STX11 directly binds resting Orai1 in the plasma membrane. (**A**) STX11 localizes in the plasma membrane. Representative confocal images of HEK293 cells expressing internal-HA-tagged STX11, stained using anti-HA antibody followed by alpaca VHH anti-rabbit secondary nanobody. Scale bar 15um. (N=3) (**B**) Co-localization of STX11 and Orai1 in the plasma membrane. Representative confocal images of HEK293 cells expressing Orai1-YFP and STX11, stained using anti-STX11 antibody followed by donkey anti-rabbit secondary antibody. Scale bar 10um. (N=3). (**C&D**) Co-immunoprecipitation of STX11 with Orai1. Whole cell lysates of resting and store-depleted HEK293 cells expressing either Flag-Orai1 and STX11 (**C**) or STX11 and Orai1-Myc-His (**D**) were subjected to immunoprecipitation and Western Blot using anti-Myc, anti-Flag or anti-STX11 antibodies, as indicated. (N=3) **(E)** Schematic showing key domains of STX11

and Orai1 used for *in vitro* pulldown assays. (**F**) Pull-down assay showing *in vitro* binding of His-tagged full length STX11 to MBP-tagged cytosolic domains of Orai1. MBP-tagged Orai1 fragments, expressed in *E. Coli* and immobilized on the amylose resin, were incubated with purified His-tagged STX11 protein. Post incubation, beads were washed, boiled and subjected to Western Blot analysis using anti-STX11 antibody. (Top panel) Ponceau S staining showing the input of MBP alone or MBP-tagged fragments. (Bottom panel) Western Blot using anti-STX11 antibody. (N=3) (**G**) Pull-down assay showing *in vitro* binding of His-tagged H_{abc} domain of STX11 to MBP-tagged Orai1 N- and C-termini performed as described above. (Top panel) Ponceau S staining showing the input of MBP alone or MBP-tagged Orai1 cytosolic tails. (Bottom panel) Western Blot using anti-His antibody. (N=3). (**H-I**) Representative structure of STX11 H_{abc} and Orai1 C-terminus complex after MD simulation (**H**) Sphere representation of STX11 H_{abc} (green) and Orai1 C-terminus (cyan) complex. The N-termini are highlighted in blue, and C-termini are highlighted in red (**I**) Cartoon representation of STX11-H_{abc} (green) and Orai1 C-terminus (cyan) complex highlighting the CA of terminal residues as spheres (**J**) Protein-protein interactions between the STX11 H_{abc} and the Orai1 C-terminus.

Figure 4: STX11 depletion compromises the functional assembly of Orai1 with Stim1 in ER-PM junctions. (**A-B**) Representative confocal images of resting (**A**) and store-depleted (**B**) scr and STX11 shRNA treated HEK293 cells expressing N-terminal CFP tagged Orai1 (CFP-Orai1) and C-terminal YFP tagged Stim1 (Stim1-YFP). (**C-H**) Box and whisker plots showing (**C**) Quantification of Stim1-YFP intensities inside Stim:Orai clusters of scr and STX11 shRNA treated HEK293 cells, ~8 min post store-depletion. (**D-E**) Quantification of CFP-Orai1 intensities inside (**D**) and outside (**E**) Stim1-YFP clusters of scr and STX11 shRNA treated cells, ~8 minute post store-depletion. N=3. Boundaries of the box plots represent 25^{th} and 75^{th} percentile values, horizontal line represents mean, white circle median and whiskers denote the outliers. (**F**) Quantification of total Orai1 levels in the plasma membrane of STX11 depleted cells. U2OS cells stably expressing Orai1-BBS-YFP were transduced with scr (black) or STX11 (red) shRNA, stimulated with 1uM TG, incubated with alpha-bungarotoxin alexa 647 (BTX-A647) and washed. BTX binding to surface Orai1 was measured using FACS, where binding to

wildtype HEK293 cells was used as control. (N=3). (**G-J**) Quantification of C-term tagged Orai1 (Orai1-YFP) and N-term tagged Stim1 (CFP-Stim1) inside puncta in control and STX11 depleted cells, ~6 minute post store-depletion. (**G-H**) Quantification of mean intensities of Orai1-YFP (**G**) and CFP-Stim1 (**H**) inside puncta. n=8. Quantification of mean area of Orai1-YFP (**I**) and CFP-Stim1 (**J**) puncta. The continuous and dotted lines represent mean and median respectively. *P<0.05, **P<0.01 and ***P<0.001 using two-tailed Student's *t* test. (**K)** Representative Fura-2 calcium imaging assay to measure Thapsigargin induced SOCE in Orai1-YFP and CFP-Stim1 expressing HEK293 cells treated with scr or STX11 shRNA.

Figure 5: STX11 binding to resting Orai1 allows successful gating by Stim1. (A) Representative Fura-2 calcium imaging assay to measure constitutive calcium influx in Orai1-S-S-GFP expressing control or STX11 depleted HEK293 cells. Cells were imaged in Ringer's buffer containing 0mM followed by 2mM extracellular Ca^{2+}. (**B**) Box and whisker plot showing quantification of constitutive calcium influx across experiments as shown in (**A**). N=3. (**C**) Representative images of YFP-CAD localization in Orai1-CFP expressing, control and STX11 depleted HEK293 cells. (**D**) Quantification of YFP-CAD in the plasma membrane of Orai1-CFP expressing HEK293 cells represented as % of total YFP-CAD in respective cells. (**E**) Representative Fura-2 calcium imaging assay to measure constitutive calcium influx in Orai1-CFP and YFP-CAD expressing control or STX11 depleted HEK293 cells. (**F-G**) Quantification of constitutive calcium influx in Orai1-CFP and YFP-CAD expressing cells described in **E,** at 0mM (**F**) and 2mM (**G**) extracellular Ca^{2+}. N=3. (**H**) Representative Fura-2 calcium imaging assay to measure constitutive calcium influx in Orai1-H134S mutant expressing control and STX11 depleted HEK293 cells as described in (**A**). (**I**) Quantification of constitutive calcium influx across experiments as shown in (**H**). N=3. Boundaries of the box plots in **B,D,F,G&I** represent 25^{th} and 75^{th} percentile values, horizontal line represents mean, white circle median and whiskers denote the outliers. *P<0.05, **P<0.01 and ***P<0.001 in (C-D,F-G,I) using two-tailed Student's *t* test.

Figure 6: Ionomycin rescues the cytotoxicity and gene expression defects in STX11 deficient FHLH4 patient T lymphocytes. (**A**) Sanger sequencing of the patient DNA showing deletion of a single of Adenine at the 752nd position and the resulting frameshift. (**B**) Western Blot of whole cell lysates prepared from healthy human control and FHLH4 patient PBMCs showing the relative molecular weight and abundance of the wildtype and mutant STX11 bands. (**C**) Fura-2 calcium imaging assay measuring anti-CD3 induced SOCE in wildtype and FHLH4 PBMCs. (**D**) Fura-2 calcium imaging assay measuring SOCE in wildtype and FHLH4 PBMCs expressing either empty vector (EV) or wildtype human STX11, respectively. (**E**) Representative Fura-2 calcium imaging assay measuring SOCE in wildtype PBMCs with or without ectopic expression of wildtype STX11. (**F**) Bar plot showing quantification of SOCE across multiple experiments in (**E**). N=3. (**G**) Granule release assay performed on the *in vitro* cultured healthy human control and FHLH4 patient CD8 T cells. PBMCs isolated from control and FHLH4 patient blood were stimulated with (2ug/ml) PHA for 48 hours. On the day of assay, cells were washed and either left unstimulated or restimulated with plate coated anti-CD3 + soluble anti-CD28 or PMA + Ionomycin in the presence of CD107a-PE antibody, stained with anti-CD8 antibody and analyzed. (N=2) (**H**) Quantification of the granule release assays as shown in (**G**). (**I**) Analysis of IL-2 expression in control and FHLH4 T cells. *In vitro* cultured healthy human control and FHLH4 patient T cells were rested and stimulated with either plate coated anti-CD3 + soluble anti-CD28 or PMA + Ionomycin for 6 hours. Total RNA was extracted and subjected to quantitative PCR analysis using Taqman probes for IL-2 and beta-actin in triplicates. *P<0.05; **P<0.01; ***P<0.001 using two-tailed Student's *t*-test.

Figure 7: Hypothetical model showing Orai1 bound to STX11 for its priming. Blue ribbons depict Orai1 in plasma membrane (PM). Green and Orange ribbons represent H_{abc} and SNARE domains of STX11, respectively. Also shown are the C-terminal cysteines of STX11 which facilitate membrane attachment of the protein.

Movies 1-3: Three independent molecular dynamic simulations of Orai1 C-terminus interaction with STX11 H_{abc} domain. Due to BioRxiv file size limit, the

movies can be found at the following link:

https://www.dropbox.com/scl/fo/3j07d3sua4g58w3yfmyv7/AAKjvIiniA-z994hxV9DNHo?rlkey=e7yj5wyukvwg5seg1awkuctc4&st=z6vp57dr&dl=0

References:

1. Clapham, D.E. Calcium signaling. *Cell* **131**, 1047-1058 (2007).
2. Vig, M. & Kinet, J.P. The long and arduous road to CRAC. *Cell Calcium* **42**, 157-162 (2007).
3. Vig, M. *et al.* Defective mast cell effector functions in mice lacking the CRACM1 pore subunit of store-operated calcium release-activated calcium channels. *Nat Immunol* **9**, 89-96 (2008).
4. Vig, M. & Kinet, J.P. Calcium signaling in immune cells. *Nat Immunol* **10**, 21-27 (2009).
5. Maul-Pavicic, A. *et al.* ORAI1-mediated calcium influx is required for human cytotoxic lymphocyte degranulation and target cell lysis. *Proc Natl Acad Sci U S A* **108**, 3324-3329 (2011).
6. Vig, M. *et al.* CRACM1 multimers form the ion-selective pore of the CRAC channel. *Curr Biol* **16**, 2073-2079 (2006).
7. Prakriya, M. & Lewis, R.S. Store-Operated Calcium Channels. *Physiol Rev* **95**, 1383-1436 (2015).
8. Soboloff, J., Rothberg, B.S., Madesh, M. & Gill, D.L. STIM proteins: dynamic calcium signal transducers. *Nat Rev Mol Cell Biol* **13**, 549-565 (2012).
9. Roos, J. *et al.* STIM1, an essential and conserved component of store-operated Ca2+ channel function. *J Cell Biol* **169**, 435-445 (2005).
10. Liou, J. *et al.* STIM is a Ca2+ sensor essential for Ca2+-store-depletion-triggered Ca2+ influx. *Curr Biol* **15**, 1235-1241 (2005).
11. Zhang, S.L. *et al.* Genome-wide RNAi screen of Ca(2+) influx identifies genes that regulate Ca(2+) release-activated Ca(2+) channel activity. *Proc Natl Acad Sci U S A* **103**, 9357-9362 (2006).
12. Vig, M. *et al.* CRACM1 is a plasma membrane protein essential for store-operated Ca2+ entry. *Science* **312**, 1220-1223 (2006).
13. Feske, S. *et al.* A mutation in Orai1 causes immune deficiency by abrogating CRAC channel function. *Nature* **441**, 179-185 (2006).
14. Yoon, T.Y. & Munson, M. SNARE complex assembly and disassembly. *Curr Biol* **28**, R397-R401 (2018).
15. Zhao, M. *et al.* Mechanistic insights into the recycling machine of the SNARE complex. *Nature* **518**, 61-67 (2015).
16. Miao, Y. *et al.* An essential and NSF independent role for alpha-SNAP in store-operated calcium entry. *Elife* **2**, e00802 (2013).
17. Li, P., Miao, Y., Dani, A. & Vig, M. alpha-SNAP regulates dynamic, on-site assembly and calcium selectivity of Orai1 channels. *Mol Biol Cell* **27**, 2542-2553 (2016).
18. Miao, Y., Bhushan, J., Dani, A. & Vig, M. Na+ influx via Orai1 inhibits intracellular ATP induced mTORC2 signaling to disrupt CD4 T cell gene expression and differentiation. *Elife* **6** (2017).
19. Ramanagoudr-Bhojappa, R., Miao, Y. & Vig, M. High affinity associations with alpha-SNAP enable calcium entry via Orai1 channels. *PLoS One* **16**, e0258670 (2021).

20. Lu, Q. *et al.* Syntaxin 1A supports voltage-dependent inhibition of alpha1B Ca2+ channels by Gbetagamma in chick sensory neurons. *J Neurosci* **21**, 2949-2957 (2001).
21. Bezprozvanny, I., Scheller, R.H. & Tsien, R.W. Functional impact of syntaxin on gating of N-type and Q-type calcium channels. *Nature* **378**, 623-626 (1995).
22. Weiss, N. & Zamponi, G.W. Regulation of voltage-gated calcium channels by synaptic proteins. *Adv Exp Med Biol* **740**, 759-775 (2012).
23. Pozzi, D., Corradini, I. & Matteoli, M. The Control of Neuronal Calcium Homeostasis by SNAP-25 and its Impact on Neurotransmitter Release. *Neuroscience* **420**, 72-78 (2019).
24. Catterall, W.A. & Few, A.P. Calcium channel regulation and presynaptic plasticity. *Neuron* **59**, 882-901 (2008).
25. He, Y. *et al.* Modulation of Kv2.1 channel gating and TEA sensitivity by distinct domains of SNAP-25. *Biochem J* **396**, 363-369 (2006).
26. Cormet-Boyaka, E. *et al.* CFTR chloride channels are regulated by a SNAP-23/syntaxin 1A complex. *Proc Natl Acad Sci U S A* **99**, 12477-12482 (2002).
27. Grimm, C. *et al.* High susceptibility to fatty liver disease in two-pore channel 2-deficient mice. *Nat Commun* **5**, 4699 (2014).
28. Lin-Moshier, Y. *et al.* The Two-pore channel (TPC) interactome unmasks isoform-specific roles for TPCs in endolysosomal morphology and cell pigmentation. *Proc Natl Acad Sci U S A* **111**, 13087-13092 (2014).
29. Toft-Bertelsen, T.L., Ziomkiewicz, I., Houy, S., Pinheiro, P.S. & Sorensen, J.B. Regulation of Ca2+ channels by SNAP-25 via recruitment of syntaxin-1 from plasma membrane clusters. *Mol Biol Cell* **27**, 3329-3341 (2016).
30. Nieto-Rostro, M., Ramgoolam, K., Pratt, W.S., Kulik, A. & Dolphin, A.C. Ablation of alpha2delta-1 inhibits cell-surface trafficking of endogenous N-type calcium channels in the pain pathway in vivo. *Proc Natl Acad Sci U S A* **115**, E12043-E12052 (2018).
31. Mohrmann, R., de Wit, H., Verhage, M., Neher, E. & Sorensen, J.B. Fast vesicle fusion in living cells requires at least three SNARE complexes. *Science* **330**, 502-505 (2010).
32. Sinha, R., Ahmed, S., Jahn, R. & Klingauf, J. Two synaptobrevin molecules are sufficient for vesicle fusion in central nervous system synapses. *Proc Natl Acad Sci U S A* **108**, 14318-14323 (2011).
33. Vig, M. & Kinet, J.P. Calcium signaling in immune cells. *Nature immunology* **10**, 21-27 (2009).
34. Jahn, R. & Scheller, R.H. SNAREs--engines for membrane fusion. *Nat Rev Mol Cell Biol* **7**, 631-643 (2006).
35. Tang, B.L., Low, D.Y. & Hong, W. Syntaxin 11: a member of the syntaxin family without a carboxyl terminal transmembrane domain. *Biochem Biophys Res Commun* **245**, 627-632 (1998).
36. Dabrazhynetskaya, A. *et al.* Syntaxin 11 marks a distinct intracellular compartment recruited to the immunological synapse of NK cells to colocalize with cytotoxic granules. *J Cell Mol Med* **16**, 129-141 (2012).
37. Zhang, G. *et al.* The vesicular transporter STX11 governs ATGL-mediated hepatic lipolysis and lipophagy. *iScience* **25**, 104085 (2022).

38. Yuan, J.P. *et al.* SOAR and the polybasic STIM1 domains gate and regulate Orai channels. *Nature cell biology* **11**, 337-343 (2009).
39. Li, Z. *et al.* Graded activation of CRAC channel by binding of different numbers of STIM1 to Orai1 subunits. *Cell Res* **21**, 305-315 (2011).
40. Park, C.Y. *et al.* STIM1 clusters and activates CRAC channels via direct binding of a cytosolic domain to Orai1. *Cell* **136**, 876-890 (2009).
41. Hou, X., Burstein, S.R. & Long, S.B. Structures reveal opening of the store-operated calcium channel Orai. *Elife* **7** (2018).
42. Yeung, P.S. *et al.* Mapping the functional anatomy of Orai1 transmembrane domains for CRAC channel gating. *Proc Natl Acad Sci U S A* **115**, E5193-E5202 (2018).
43. Zhang, K. *et al.* Familial Hemophagocytic Lymphohistiocytosis, in *GeneReviews((R))*. (eds. M.P. Adam *et al.*) (Seattle (WA); 1993).
44. Hou, X., Pedi, L., Diver, M.M. & Long, S.B. Crystal structure of the calcium release-activated calcium channel Orai. *Science* **338**, 1308-1313 (2012).
45. Jessen, B. *et al.* Graded defects in cytotoxicity determine severity of hemophagocytic lymphohistiocytosis in humans and mice. *Front Immunol* **4**, 448 (2013).
46. Chinn, I.K. *et al.* Genetic and mechanistic diversity in pediatric hemophagocytic lymphohistiocytosis. *Blood* **132**, 89-100 (2018).
47. Zhizhuo, H. *et al.* Screening the PRF1, UNC13D, STX11, SH2D1A, XIAP, and ITK gene mutations in Chinese children with Epstein-Barr virus-associated hemophagocytic lymphohistiocytosis. *Pediatr Blood Cancer* **58**, 410-414 (2012).
48. Hellewell, A.L., Foresti, O., Gover, N., Porter, M.Y. & Hewitt, E.W. Analysis of familial hemophagocytic lymphohistiocytosis type 4 (FHL-4) mutant proteins reveals that S-acylation is required for the function of syntaxin 11 in natural killer cells. *PLoS One* **9**, e98900 (2014).
49. Hackmann, Y. *et al.* Syntaxin binding mechanism and disease-causing mutations in Munc18-2. *Proc Natl Acad Sci U S A* **110**, E4482-4491 (2013).
50. Neveu, E., Khalifeh, D., Salamin, N. & Fasshauer, D. Prototypic SNARE Proteins Are Encoded in the Genomes of Heimdallarchaeota, Potentially Bridging the Gap between the Prokaryotes and Eukaryotes. *Curr Biol* **30**, 2468-2480 e2465 (2020).

Acknowledgements: We thank Vivien Beziat, Yenan Bryceson, Heinrich Schlums, Jelve Nejati Zendegani, Stephan Ehl, and Jasmin Mann for help with human PBMC handling, isolation, storage and shipping. Anand Vaidya for advice on STX11 purification. Jyoti Rohilla for technical support. This work was supported in part by Department of Atomic Energy, Government of India under Project Identification No. RTI 4007 and NIH-NIAID grant AI108636.

Figure 1

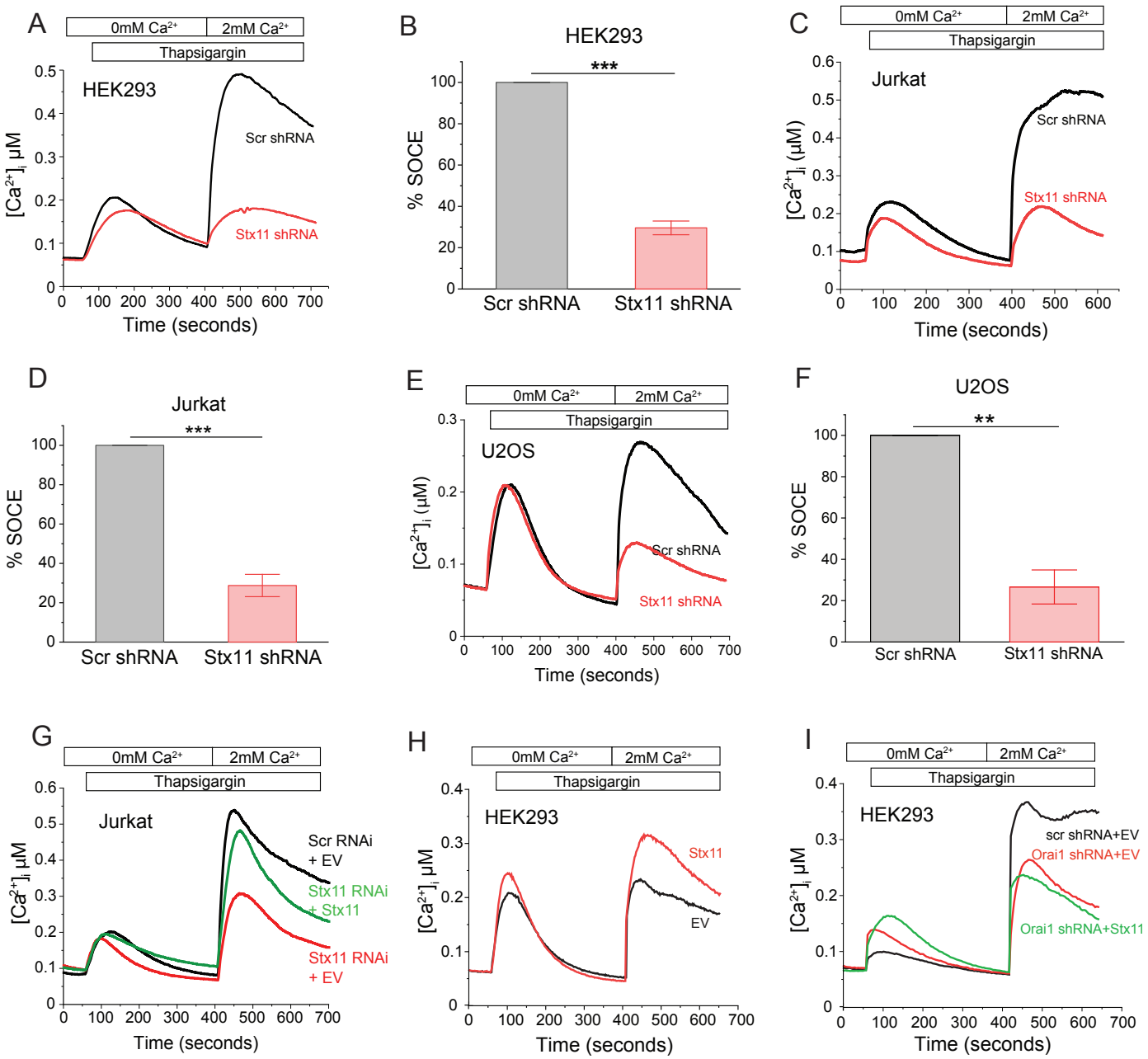

Figure 1: STX11 is required for SOCE.
(A-F) RNAi mediated depletion of STX11 reduces SOCE. Measurement of thapsigargin (TG) induced SOCE in various cell lines after shRNA mediated depletion of STX11. The traces in panels A,C,E show representative average single cell Fura-2 calcium imaging assays. Bars in panels B,D,F show mean % SOCE SE from three independent experiments each where mean SOCE from scramble (scr) shRNA treated group in each experiment was set at 100% and the relative response of STX11 shRNA treated groups was calculated respectively. *P<0.05; **P<0.01; ***P<0.001 using two-tailed Student's t test. (G) Representative Fura-2 calcium imaging assay showing reconstitution of SOCE in STX11 depleted Jurkat T cells by ectopic expression of STX11. Black (scr shRNA), red (STX11 shRNA), green (STX11 shRNA with STX11 expression). N=2 (H) Ectopic expression of STX11 enhances SOCE. Representative Fura-2 calcium imaging assay showing SOCE in HEK293 cells expressing STX11 (red) or empty vector (EV) (black). (N=3) (I) STX11 mediated enhancement of SOCE is dependent on Orai1. A representative Fura 2 calcium imaging assay showing measurement of thapsigargin (TG) induced SOCE in HEK293 cells where Orai1 expression was depleted using shRNA and STX11 was over-expressed. (N=2)

Figure 2

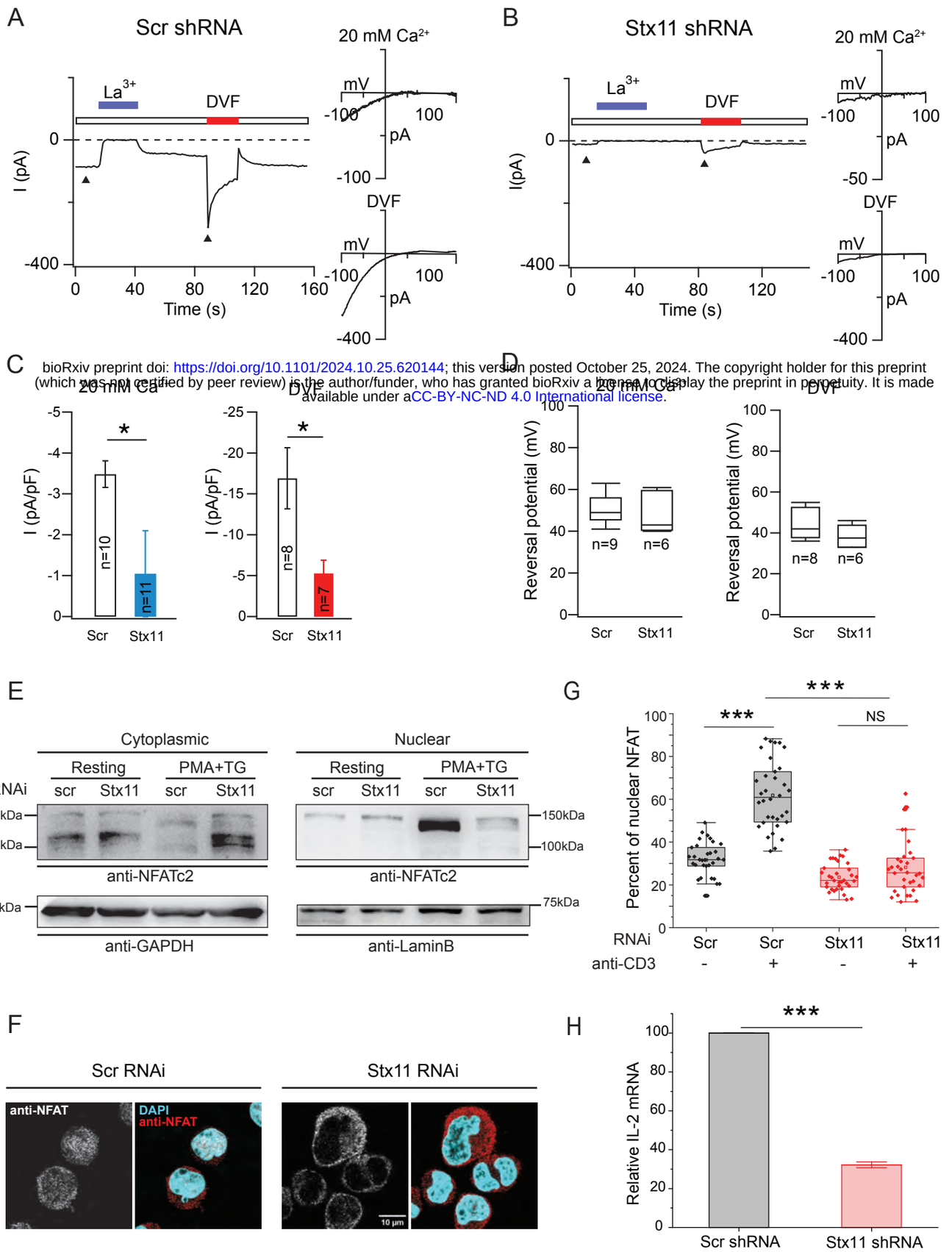

Figure 2: STX11 depletion suppresses ICRAC, downstream signaling and gene expression in Jurkat T cells. ICRAC was recorded from Jurkat T-cells in the whole-cell recording configuration in 20 mM extracellular Ca2+ Ringer's solution. ICRAC was induced by passive depletion of intracellular Ca2+ stores by dialyzing 8 mM BAPTA into the cell via the patch-pipette. (A) Representative current at -100 mV in Jurkat T cell transfected with scr shRNA construct. The current is blocked by extracellular La3+ (100 µM) and replacing the 20 mM Ca2+ Ringer's solution with a divalent free solution (DVF) evokes a large Na+ current which depotentiates over tens of seconds. The current-voltage (I-V) relationship of the Ca2+ and DVF currents are shown on the right. (B) ICRAC from a Jurkat T cell transfected with STX11 shRNA. Both Ca2+ and Na+ current amplitudes are reduced relative to control cells. The I-V relationships (right plots) show no change in ion selectivity. (C-D) Summary of the current amplitudes of Ca2+ and Na+ currents and current reversal potentials in scr and STX11 knockdown cells. (E&F) Estimation of nuclear translocation of NFAT. (E) Western Blot showing nuclear translocation of NFAT in Jurkat T cells treated with scr or STX11 shRNA for 4 days and stimulated with PMA+TG for 30min prior to the preparation of nuclear and cytoplasmic extracts. (N=3) (F) Representative confocal images of Jurkat T cells treated with scr or STX11 shRNA for 4 days and stimulated with 10ug/ml anti-CD3 for 1 hour. Following stimulation, cells were fixed, permeabilized and stained using anti-NFAT primary antibody, followed by donkey anti-rabbit AF647 secondary antibody, and counter-stained with DAPI to mark the nuclei. (N=2) (G) Box and whisker plot showing percent nuclear NFAT in Jurkat T cells quantified from 40-50 cells populating 10 randomly chosen fields per group in (F). Boundaries of the box plots represent 25th and 75th percentile values, horizontal line represents mean, white circle represents median and whiskers denote the outliers. (H) Quantitative PCR to assess IL-2 transcription in anti-CD3 stimulated Jurkat T cells. Jurkat T cells were treated with scr or STX11 shRNA for 4 days and stimulated with 5ug/ml anti-CD3 for 3 hours. Total RNA was extracted from cells and subjected to QPCR analysis using Taqman probes for IL-2 and beta-actin. The bars show relative IL-2 mRNA expression levels with the scr shRNA treated group set at 100%. Shown here are mean SE. (N=3) (F-H) *P<0.05; **P<0.01; ***P<0.001 using two-tailed Student's t test.

Figure 3

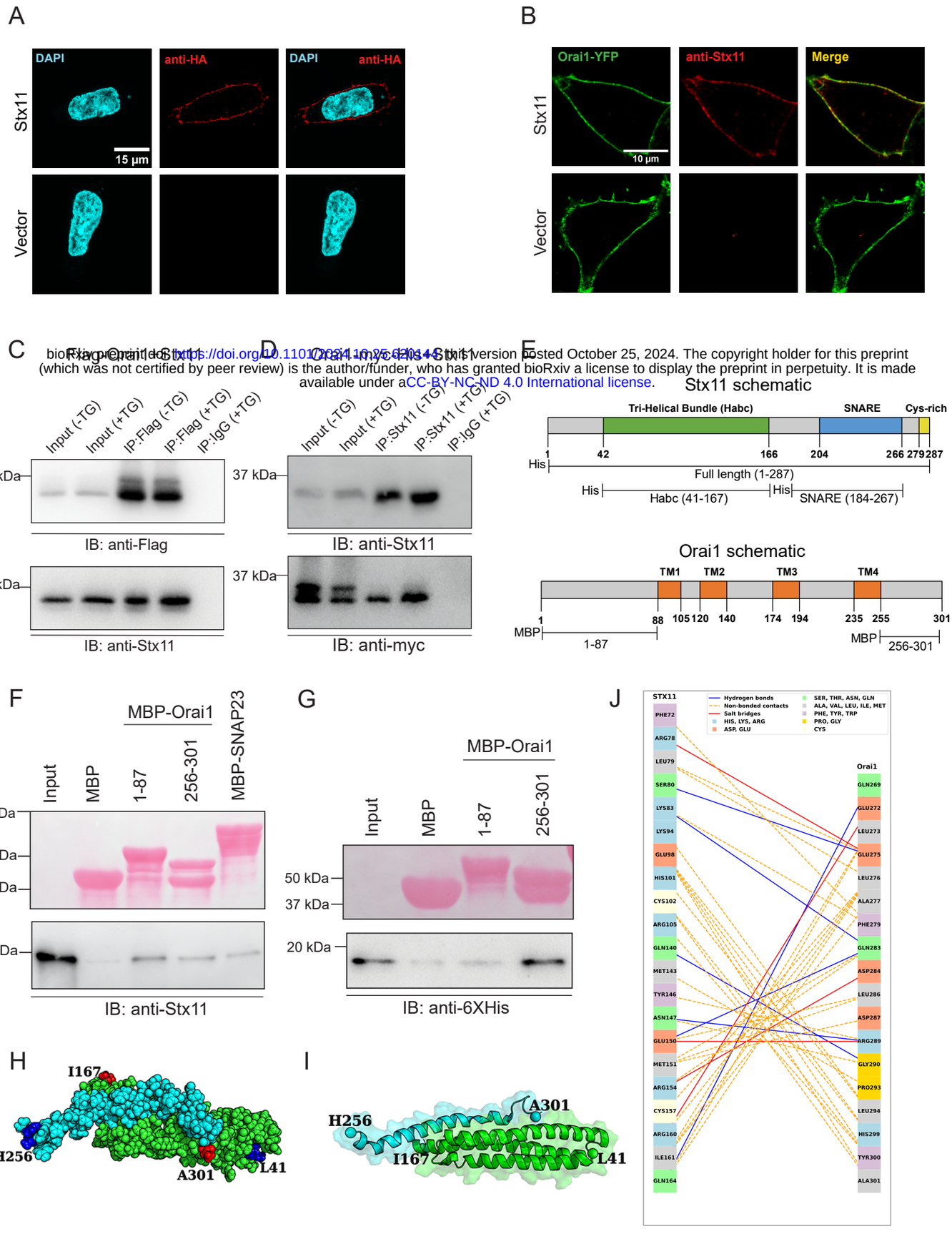

Figure 3: STX11 directly binds resting Orai1 in the plasma membrane. (A) STX11 localizes in the plasma membrane. Representative confocal images of HEK293 cells expressing internal-HA-tagged STX11, stained using anti-HA antibody followed by alpaca VHH anti-rabbit secondary nanobody. Scale bar 15um. (N=3) (B) Co-localization of STX11 and Orai1 in the plasma membrane. Representative confocal images of HEK293 cells expressing Orai1-YFP and STX11, stained using anti-STX11 antibody followed by donkey anti-rabbit secondary antibody. Scale bar 10um. (N=3). (C&D) Co-immunoprecipitation of STX11 with Orai1. Whole cell lysates of resting and store-depleted HEK293 cells expressing either Flag-Orai1 and STX11 (C) or STX11 and Orai1-Myc-His (D) were subjected to immunoprecipitation and Western Blot using anti-Myc, anti-Flag or anti-STX11 antibodies, as indicated. (N=3) (E) Schematic showing key domains of STX11 and Orai1 used for in vitro pulldown assays. (F) Pull-down assay showing in vitro binding of His-tagged full length STX11 to MBP-tagged cytosolic domains of Orai1. MBP-tagged Orai1 fragments, expressed in E. Coli and immobilized on the amylose resin, were incubated with purified His-tagged STX11 protein. Post incubation, beads were washed, boiled and subjected to Western Blot analysis using anti-STX11 antibody. (Top panel) Ponceau S staining showing the input of MBP alone or MBP-tagged fragments. (Bottom panel) Western Blot using anti-STX11 antibody. (N=3) (G) Pull-down assay showing in vitro binding of His-tagged Habc domain of STX11 to MBP-tagged Orai1 N- and C-termini performed as described above. (Top panel) Ponceau S staining showing the input of MBP alone or MBP-tagged Orai1 cytosolic tails. (Bottom panel) Western Blot using anti-His antibody. (N=3). (H-I) Representative structure of STX11 Habc and Orai1 C-terminus complex after MD simulation (H) Sphere representation of STX11 Habc (green) and Orai1 C-terminus (cyan) complex. The N-termini are highlighted in blue, and C-termini are highlighted in red (I) Cartoon representation of STX-11-Habc (green) and Orai1 C-terminus (cyan) complex highlighting the CA of terminal residues as spheres (J) Protein-protein interactions between the STX11 Habc and the Orai1 C-terminus.

Figure 4

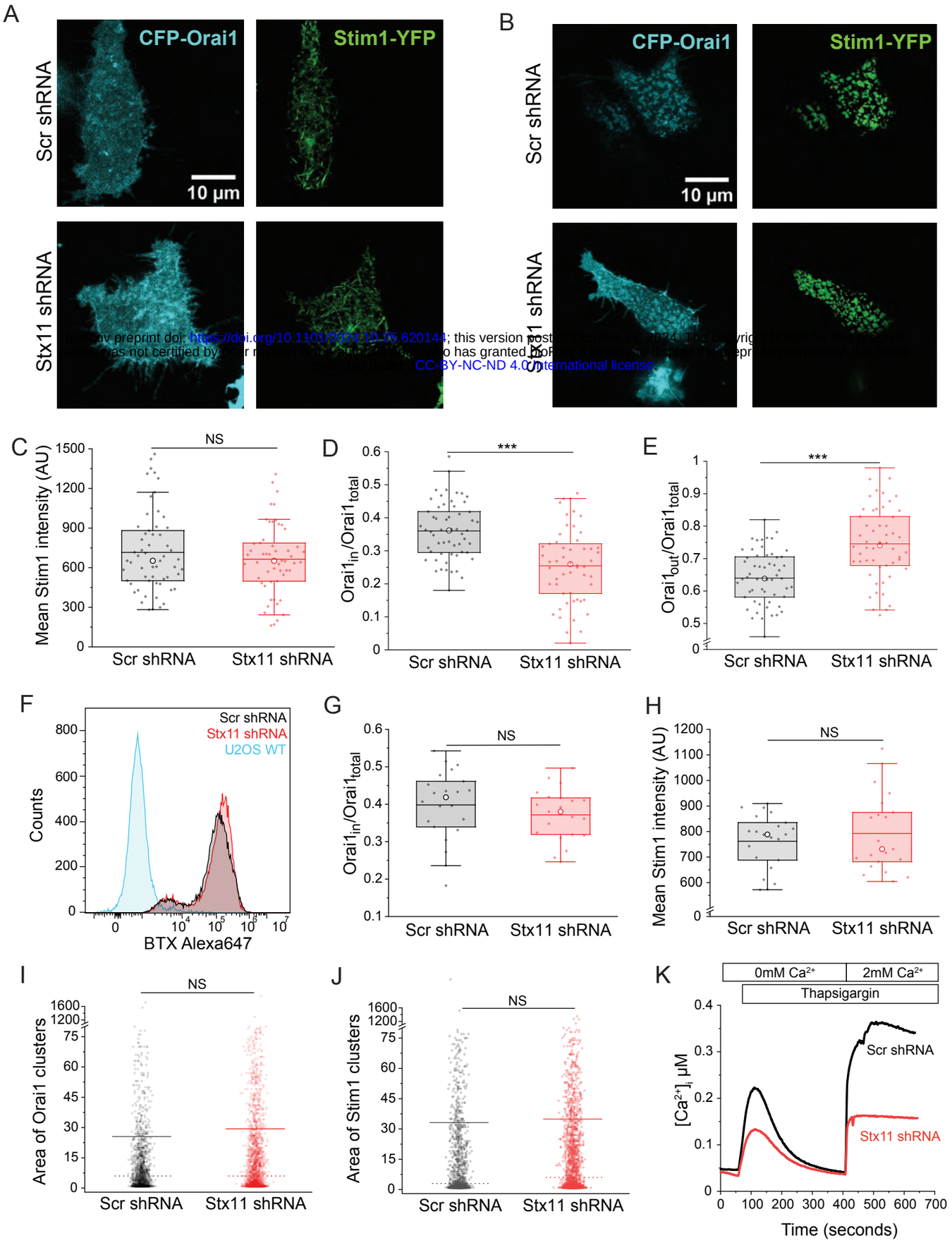

Figure 4: STX11 depletion compromises the functional assembly of Orai1 with Stim1 in ER-PM junctions. (A-B) Representative confocal images of resting (A) and store-depleted (B) scr and STX11 shRNA treated HEK293 cells expressing N-terminal CFP tagged Orai1 (CFP-Orai1) and C-terminal YFP tagged Stim1 (Stim1-YFP). (C-H) Box and whisker plots showing (C) Quantification of Stim1-YFP intensities inside Stim:Orai clusters of scr and STX11 shRNA treated HEK293 cells, ~8 min post store-depletion. (D-E) Quantification of CFP-Orai1 intensities inside (D) and outside (E) Stim1-YFP clusters of scr and STX11 shRNA treated cells, ~8 minute post store-depletion. N=3. Boundaries of the box plots represent 25th and 75th percentile values, horizontal line represents mean, white circle median and whiskers denote the outliers. (F) Quantification of total Orai1 levels in the plasma membrane of STX11 depleted cells. U2OS cells stably expressing Orai1-BBS-YFP were transduced with scr (black) or STX11 (red) shRNA, stimulated with 1uM TG, incubated with alpha-bungarotoxin alexa 647 (BTX-A647) and washed. BTX binding to surface Orai1 was measured using FACS, where binding to wildtype HEK293 cells was used as control. (N=3). (G-J) Quantification of C-term tagged Orai1 (Orai1-YFP) and N-term tagged Stim1 (CFP-Stim1) inside puncta in control and STX11 depleted cells, ~6 minute post store-depletion. (G-H) Quantification of mean intensities of Orai1-YFP (G) and CFP-Stim1 (H) inside puncta. n=8. Quantification of mean area of Orai1-YFP (I) and CFP-Stim1 (J) puncta. The continuous and dotted lines represent mean and median respectively. *P<0.05, **P<0.01 and ***P<0.001 using two-tailed Student's t test. (K) Representative Fura-2 calcium imaging assay to measure Thapsigargin induced SOCE in Orai1-YFP and CFP-Stim1 expressing HEK293 cells treated with scr or STX11 shRNA.

Figure 5

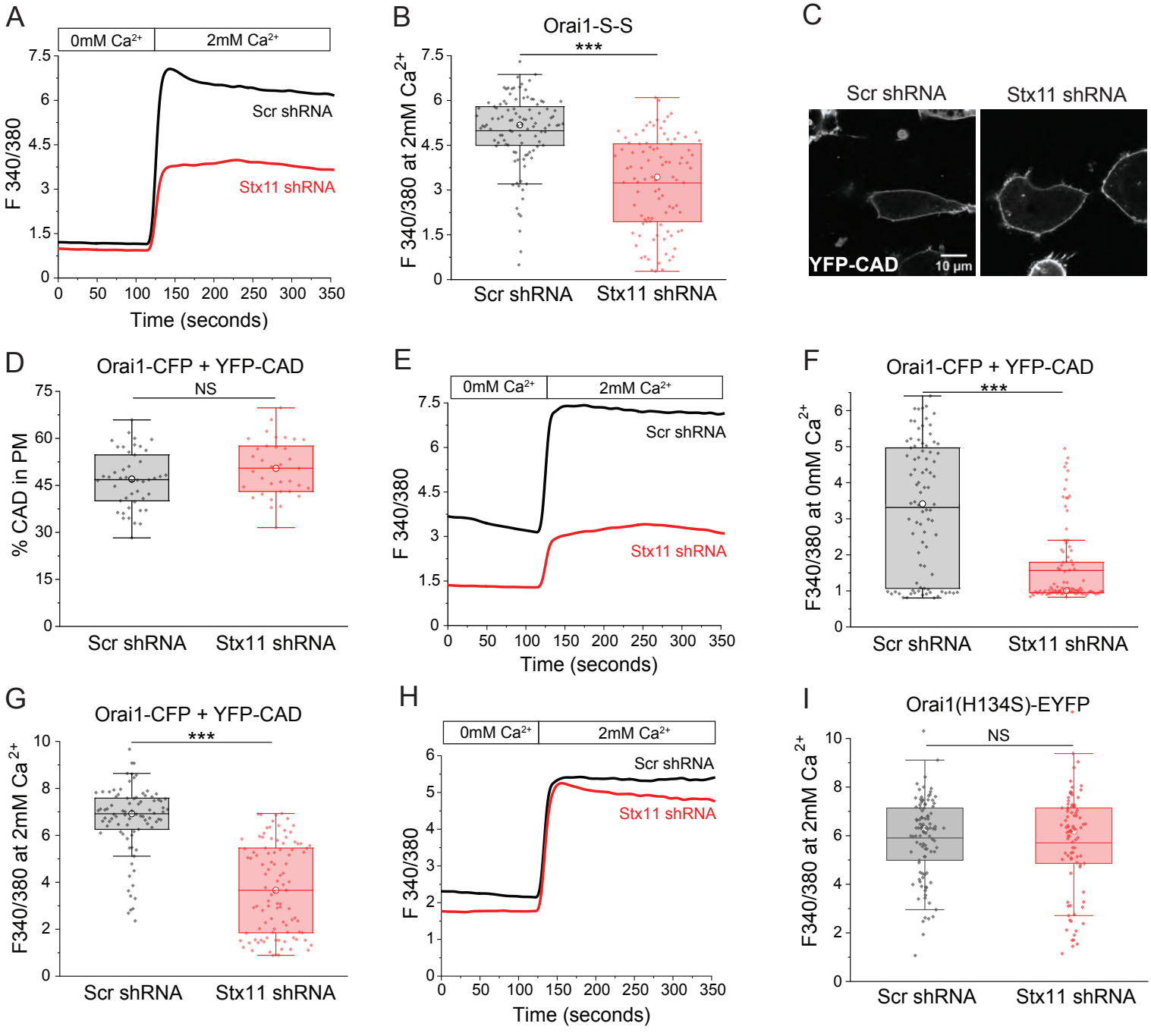

Figure 5: STX11 binding to resting Orai1 allows successful gating by Stim1. (A) Representative Fura-2 calcium imaging assay to measure constitutive calcium influx in Orai1-S-S-GFP expressing control or STX11 depleted HEK293 cells. Cells were imaged in Ringer's buffer containing 0mM followed by 2mM extracellular Ca2+. (B) Box and whisker plot showing quantification of constitutive calcium influx across experiments as shown in (A). N=3. (C) Representative images of YFP-CAD localization in Orai1-CFP expressing, control and STX11 depleted HEK293 cells. (D) Quantification of YFP-CAD in the plasma membrane of Orai1-CFP expressing HEK293 cells represented as % of total YFP-CAD in respective cells. (E) Representative Fura-2 calcium imaging assay to measure constitutive calcium influx in Orai1-CFP and YFP-CAD expressing control or STX11 depleted HEK293 cells. (F-G) Quantification of constitutive calcium influx in Orai1-CFP and YFP-CAD expressing cells described in E, at 0mM (F) and 2mM (G) extracellular Ca2+. N=3. (H) Representative Fura-2 calcium imaging assay to measure constitutive calcium influx in Orai1-H134S mutant expressing control and STX11 depleted HEK293 cells as described in (A). (I) Quantification of constitutive calcium influx across experiments as shown in (H). N=3. Boundaries of the box plots in B,D,F,G&I represent 25th and 75th percentile values, horizontal line represents mean, white circle median and whiskers denote the outliers. *P<0.05, **P<0.01 and ***P<0.001 in (C-D,F-G,I) using two-tailed Student's t test.

Figure 6

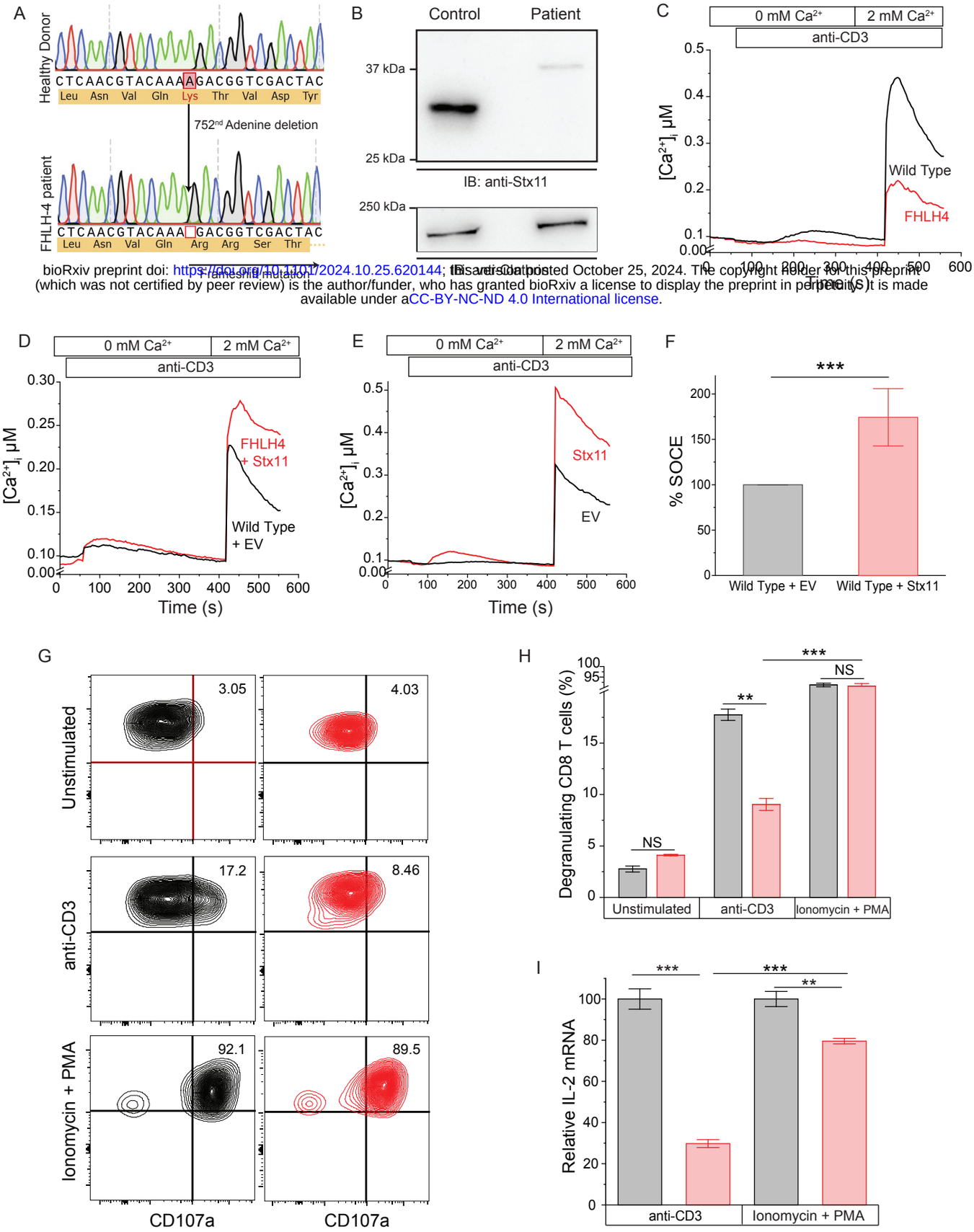

Figure 6: Ionomycin rescues the cytotoxicity and gene expression defects in STX11 deficient FHLH4 patient T lymphocytes. (A) Sanger sequencing of the patient DNA showing deletion of a single of Adenine at the 752nd position and the resulting frameshift. (B) Western Blot of whole cell lysates prepared from healthy human control and FHLH4 patient PBMCs showing the relative molecular weight and abundance of the wildtype and mutant STX11 bands. (C) Fura-2 calcium imaging assay measuring anti-CD3 induced SOCE in wildtype and FHLH4 PBMCs. (D) Fura-2 calcium imaging assay measuring SOCE in wildtype and FHLH4 PBMCs expressing either empty vector (EV) or wildtype human STX11, respectively. (E) Representative Fura-2 calcium imaging assay measuring SOCE in wildtype PBMCs with or without ectopic expression of wildtype STX11. (F) Bar plot showing quantification of SOCE across multiple experiments in (E). N=3. (G) Granule release assay performed on the in vitro cultured healthy human control and FHLH4 patient CD8 T cells. PBMCs isolated from control and FHLH4 patient blood were stimulated with (2ug/ml) PHA for 48 hours. On the day of assay, cells were washed and either left unstimulated or restimulated with plate coated anti-CD3 + soluble anti-CD28 or PMA + Ionomycin in the presence of CD107a-PE antibody, stained with anti-CD8 antibody and analyzed. (N=2) (H) Quantification of the granule release assays as shown in (G). (I) Analysis of IL-2 expression in control and FHLH4 T cells. In vitro cultured healthy human control and FHLH4 patient T cells were rested and stimulated with either plate coated anti-CD3 + soluble anti-CD28 or PMA + Ionomycin for 6 hours. Total RNA was extracted and subjected to quantitative PCR analysis using Taqman probes for IL-2 and beta-actin in triplicates. *P<0.05; **P<0.01; ***P<0.001 using two-tailed Student's t-test.

Figure 7

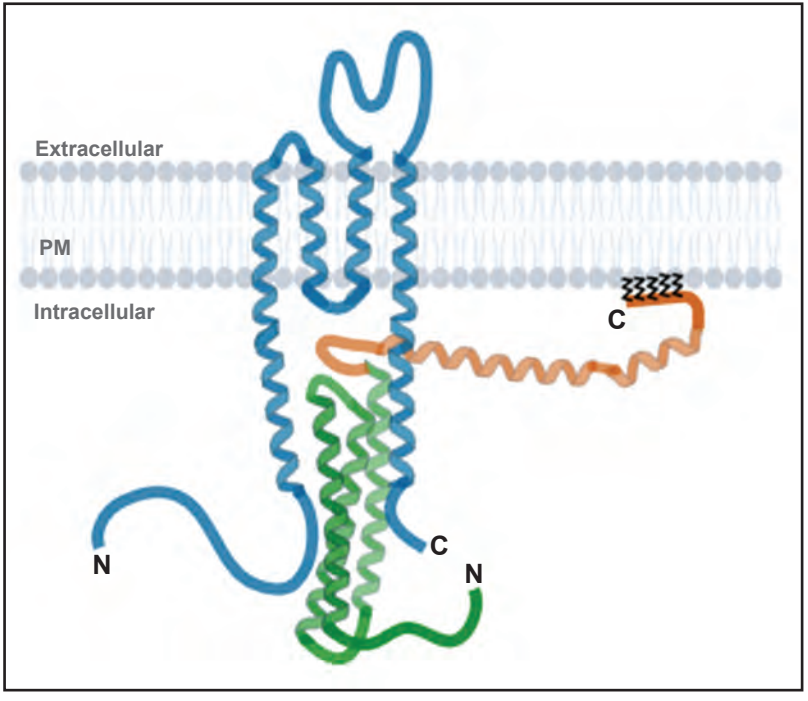

Figure 7: Hypothetical model showing Orai1 bound to STX11 for its priming. Blue ribbons depict Orai1 in plasma membrane (PM). Green and Orange ribbons represent Habc and SNARE domains of STX11, respectively. Also shown are the C-terminal cysteines of STX11 which facilitate membrane attachment of the protein.